RESEARCH ARTICLE

Frederick Otu-Larbi and Kirsti Ashworth joint first authors.

Key Points:
- Medlyn coupled stomatal conductance-photosynthesis model best reproduces observed plant productivity (GPP) across various ecosystems
- Modeled GPP and stomatal conductance across forest ecosystems differ by up to a factor of 3 between different model configurations
- Ozone deposition rates could vary by ∼13% depending on stomatal conductance model used with implications for estimated tropospheric ozone

Supporting Information:
Supporting Information may be found in the online version of this article.

Correspondence to:
K. Ashworth,
k.s.ashworth1@lancaster.ac.uk

FORCAsT-gs: Importance of Stomatal Conductance Parameterization to Estimated Ozone Deposition Velocity

Frederick Otu-Larbi[1] , Adriano Conte[2], Silvano Fares[2,3] , Oliver Wild[1] , and Kirsti Ashworth[1]

[1]Lancaster Environment Centre, Lancaster University, Lancaster, UK, [2]Council for Agricultural Research and Economics (CREA)–Research Centre for Forestry and Wood, Arezzo, Italy, [3]National Research Council of Italy–Institute of BioEconomy, Rome, Italy

Abstract The role of stomata in regulating photosynthesis and transpiration, and hence governing global biogeochemical cycles and climate, is well-known. Less well-understood, however, is the importance of stomatal control to the exchange of other trace gases between terrestrial vegetation and the atmosphere. Yet these gases determine atmospheric composition, and hence air quality and climate, on scales ranging from local to global, and seconds to decades. Vegetation is a major sink for ground-level ozone via the process of dry deposition and the primary source of many biogenic volatile organic compounds (BVOCs). The rate of dry deposition is largely controlled by the rate of diffusion of a gas through the stomata, and this also governs the emission rate of some key BVOCs. It is critical therefore that canopy-atmosphere exchange models capture the physiological processes controlling stomatal conductance and the transfer of trace gases other than carbon dioxide and water vapor. We incorporate three of the most widely used coupled stomatal conductance-photosynthesis models into the one-dimensional multi-layer FORest Canopy-Atmosphere Transfer (FORCAsT1.0) model to assess the importance of choice of parameterization on simulated ozone deposition rates. Modeled GPP and stomatal conductance across a broad range of ecosystems differ by up to a factor of two between the best and worst performing model configurations. This leads to divergences in seasonal and diel profiles of ozone deposition velocity of up to 30% and deposition rate of up to 13%, demonstrating that the choice of stomatal conductance parameterization is critical in accurate quantification of ozone deposition.

Plain Language Summary Plants open and close their stomata to regulate the uptake of carbon dioxide (photosynthesis) and the release of water vapor into the atmosphere. Trace gases like ozone can also enter the stomata causing damage to leaves, reducing plant growth and productivity in the process. Stomatal conductance, the measure of stomatal opening, is therefore important for assessing the concentration of ozone in the atmosphere and the impacts of pollutants on plants. It is critical that canopy-atmosphere exchange models capture the processes controlling stomatal conductance and the transfer of trace gases other than carbon dioxide and water vapor. We incorporate three widely used coupled stomatal conductance-photosynthesis models into a 1-Dimensional multi-layer model to assess how the choice of model parameters affect the rate at which ozone is deposited onto plant surfaces. We first validate the model using observations from various forests sites and then compare ozone deposition rates between the best and worst performing model at each site. We find that ozone deposition rates can vary by up 13% in response to changes in model parameters, demonstrating that the choice of stomatal conductance parameterization is crucial in understanding ozone deposition, a major process through which ozone is removed from the troposphere.

1. Introduction

Photosynthesis and transpiration of the world's forests drive the carbon, hydrological and nutrient cycles, governing climate, ecosystem health and productivity, and biodiversity. Forests also serve as a sink for trace gases which are deposited onto plant surfaces and taken up through the stomata. Dry deposition of ozone is of particular importance as it represents a major sink of this tropospheric pollutant. It is also of particular concern because ozone can damage photosynthetic apparatus limiting growth and productivity. The rates of photosynthesis and uptake of ozone are both dependent on the degree of stomatal opening, referred to as stomatal conductance. Plants open and close the stomata to maintain a balance between photosynthesis

Author Contributions:
Conceptualization: Frederick Otu-Larbi, Adriano Conte, Silvano Fares, Oliver Wild, Kirsti Ashworth
Formal analysis: Frederick Otu-Larbi, Kirsti Ashworth
Funding acquisition: Oliver Wild, Kirsti Ashworth
Methodology: Frederick Otu-Larbi, Adriano Conte, Silvano Fares, Oliver Wild, Kirsti Ashworth
Visualization: Frederick Otu-Larbi
Writing – original draft: Frederick Otu-Larbi
Writing – review & editing: Frederick Otu-Larbi, Adriano Conte, Silvano Fares, Oliver Wild, Kirsti Ashworth

(CO_2 uptake) and leaf transpiration (water loss), thereby regulating the exchange of CO_2 and water vapor between vegetation and the atmosphere (Hetherington & Woodward, 2003).

Gases and particles deposited on leaf surfaces may be taken up through the stomata or cuticle into the leaf tissue. Stomatal uptake is the dominant of these routes for most reactive trace gases like ozone (Royal Society, 2008). The rate of stomatal diffusion and uptake is dependent on both the diffusivity of the gas and the size of the stomata: the wider the stomatal aperture the lower the resistance to diffusion through the stomata. As gases diffuse through the stomata, their concentrations are reduced at the leaf surface, increasing the concentration gradient between the leaf and the atmosphere above it. This concentration gradient also drives deposition–the greater the gradient the higher the deposition velocity. Total deposition rates are therefore dependent both directly and indirectly on stomatal conductance.

Ozone taken up through stomata is detrimental to plant growth and health leading to a decrease in productivity, causing billions of dollars in crop losses annually (Ainsworth et al., 2012; Avnery et al., 2011). Ozone damage has been shown to reduce gross primary productivity (GPP) by up to 10% in different forest ecosystems under current climatic conditions, although this impact is projected to decline in future as increased CO_2 and drought severity reduce stomatal conductance and hence stomatal ozone uptake (Oliver et al., 2018; Otu-Larbi, Conte, et al., 2020).

Stomatal conductance is a key factor controlling ozone deposition velocity and deposition rates, and therefore the extent and severity of damage. It is critical that models that couple the land surface and the atmosphere are able to accurately reproduce stomatal conductance in order to account fully for the processes driving photosynthesis and trace gas deposition rates. Many empirical and semi-empirical approaches have been developed to simulate stomatal conductance. One of the earliest and most widely used is a multiplicative model (Jarvis, 1976) which reduces stomatal conductance from its potential maximum according to observed responses to changing environmental conditions. Each environmental influence is assumed independent of the others (Damour et al., 2010) and the approach does not consider physiological interactions or feedbacks that could alter stomatal movement (Yu et al., 2004). Subsequent research demonstrated that stomatal aperture was also directly regulated by current photosynthesis rate (Wong et al., 1979) leading to the development of semi-empirical coupled models that assume a linear relationship between photosynthesis (An) and gs, and iterate to simultaneously solve for both (e.g., Ball et al., 1987). More recently, optimisation theory has been applied to these coupled photosynthesis-stomatal conductance models to replicate the "regulatory" role of stomata, that is, that plants control stomatal aperture to maximize carbon gain while minimizing water loss (Cowan & Farquhar, 1977; Medlyn et al., 2011).

These model formulations adopt different approaches to account for the impacts on stomatal conductance of environmental factors such as drought, and physiological factors such as phenology. Each requires specific parameters which can be difficult to obtain for particular species and climates leading to the use of generic values for similar plant functional types. As estimates of stomatal conductance are sensitive to both model formulation and parameter value there are large uncertainties associated with modeled stomatal conductance and photosynthesis rates. Interestingly though, some studies report little difference between conductance estimated based on optimisation theory and semi-empirical methods, suggesting that for some species and ecosystems the choice of model formulation is not a major factor in determining model performance (Franks et al., 2017, 2018).

The multi-layer canopy-atmosphere model FORCAsT1.0 (FORest Canopy-Atmosphere Transfer) was initially developed as an atmospheric chemistry tool for upscaling leaf-level biogenic emissions to the canopy scale and interpreting measurement data from intensive field campaigns at forest sites (CACHE; Forkel et al., 2006). It has since been modified to better capture observed dynamics and turbulent transport (CACHE; Bryan et al., 2012) and to reflect our improved understanding of the atmospheric chemistry of biogenic volatiles, particularly in low-NOx environments (FORCAsT1.0; Ashworth et al., 2015). Parameterisations of the response of isoprene emissions to water stress and re-wetting have also been incorporated into the model and demonstrated to improve model reproduction of changes in isoprene concentrations at a temperate deciduous woodland during an extended heatwave-drought (Otu-Larbi, Bolas, et al., 2020).

The model has demonstrated considerable skill in reproducing observed concentrations and fluxes of short-lived biogenic reactive trace gases and their products over short time periods at a number of Northern

Hemisphere forest sites (Ashworth et al., 2015; Bryan et al., 2012, 2015; Forkel et al., 2006). However, production outweighs loss processes for some gaseous species, suggesting that either deposition rates or vertical transport out of the canopy are too slow, or foliage emissions overestimated. These processes are dependent on the rate of gas exchange through the stomata, and hence the skill of the model in capturing stomatal conductance over time periods from minutes, to hours, to seasons.

Explicit inclusion of physiological processes in FORCAsT1.0 has the additional benefit of enabling model performance to be evaluated against canopy-scale photosynthesis and transpiration (represented by canopy-top fluxes of CO_2 and water vapor) which are routinely measured and readily available over long time periods across a wide range of ecosystems. This allows a more thorough exploration and constraint of the physical and dynamical processes occurring within the canopy than is possible from concentration and flux measurements of short-lived reactive species made during short intensive field campaigns. Constraining these processes would allow us to focus more closely on the mechanisms of the production and loss of short-lived atmospherically relevant biogenic trace gases.

We incorporate three parameterisations of stomatal conductance and photosynthesis into FORCAsT1.0 to assess:

1. the ability of different coupled stomatal conductance-photosynthesis models to reproduce observed CO_2 fluxes across a range of different forest ecosystems and climate regions
2. the divergence of simulated ozone deposition velocities and deposition rates due to differences in stomatal conductance modeling approach and parameterization

We use observation data from five forest sites within the FLUXNET2015 data set (Pastorello et al., 2020), the most comprehensive high-quality data available from worldwide flux networks, to evaluate the performance of each of the three stomatal conductance-photosynthesis models. The sites cover three different forest ecosystems classified by the International Geosphere-Biosphere Program (IGBP) as Evergreen Broadleaf Forests (EBF), Evergreen Needleleaf Forests (ENF) and Deciduous Broadleaf Forests (DBF), and three climate regions: boreal, temperate and tropical, with two of the temperate sites further sub-classified as Mediterranean. Our ultimate goal is to understand and quantify the uncertainties in modeled gross primary productivity and ozone deposition rates due to the choice of stomatal conductance model and model parameters.

2. Methods

2.1. FORCAsT-gs

The 1-D (vertical column) model, FORest Canopy-Atmosphere Transfer (FORCAsT1.0), was developed to simulate exchanges of reactive biogenic volatiles between a forest site and the atmospheric boundary layer. Previous versions (CACHE: Bryan et al., 2012, 2015; Forkel et al., 2006; and FORCAsT1.0: Ashworth et al., 2015; Otu-Larbi, Bolas, et al., 2020) have focused on the atmospheric processes governing the concentration and distribution of these volatiles and their oxidation products within and above the canopy. FORCAsT uses 40 vertical levels as a default, 20 of which are in the vegetation canopy space, with the remainder of the levels representing the planetary boundary layer above. The thickness of the layers increases with height, permitting greater resolution in the canopy space, which is further sub-divided into a trunk space (10 levels) and crown space (10 levels). More details about how vegetation is treated in the model can be found in Ashworth et al. (2015).

Heat and mass fluxes are calculated at each model level by solving the continuity equations, shown here for (gas-phase) mass:

$$\frac{\partial c}{\partial t} = \frac{\partial}{\partial z}\left(K\frac{\partial c}{\partial z}\right) + S_c, \tag{1}$$

where c is the concentration or mixing ratio of a chemical species or water vapor, z is the height of the layer, K is the turbulent exchange coefficient and S_c represents all sources and sinks of the species (i.e., emissions, deposition, chemical production and loss, and advection). All are explicitly parameterized within the model and have been fully described by Bryan et al. (2012) and Ashworth et al. (2015). We briefly re-cap those that

remain unchanged from FORCAsT1.0 (Ashworth et al., 2015) before fully describing the coupled stomatal conductance-photosynthesis models we have now incorporated into FORCAsT-gs.

Leaf-level volatile emissions are calculated for each foliated canopy layer in FORCAsT-gs following the light- and temperature-dependent emission algorithms developed by Guenther et al. (1995):

$$F = \text{LAI} \cdot \varepsilon \cdot \gamma_{TS} \cdot \gamma_{LS}, \tag{2}$$

where LAI is the leaf area index in each leaf-angle class and layer, ε is the emission factor or base emission rate (i.e., at standard conditions of 30°C and 1,000 μmol m^{-2} s^{-1} photosynthetically active radiation, PAR) and γ_{TS} and γ_{LS} are activity factors that scale the base emission rate according to actual temperature and PAR. For temperature-dependent-only emissions from specialized storage pools, γ_{TS} and γ_{LS} in Equation 2 is replaced by γ_{TP} based on Steinbrecher et al. (1999). Further details of the activity factors and parameters are presented in Ashworth et al. (2015). The chemistry in FORCAsT-gs is unchanged from that described by Ashworth et al. (2015). Users can use either the Regional Atmospheric Chemistry Mechanism (RACM; Geiger et al., 2003; Stockwell et al., 1997) or the Caltech Atmospheric Chemistry Mechanism (CACM; Chen et al., 2006; Griffin et al., 2003, 2005). The former includes 84 species and 249 reactions, and the latter 300 species and 630 gas-phase reactions with partitioning to aerosol via the Model to Predict the Multiphase Partitioning of Organics (MPMPO; Ashworth et al., 2015; Chen et al., 2006).

Vertical mixing in and above the canopy are based on Baldocchi (1988) and Gao et al. (1993), respectively, following first-order K-theory (Blackadar, 1962). Eddy diffusivity is constrained by friction velocity measurements made close to but just above the top of the canopy as K-theory breaks down in the highly turbulent canopy sub-layer (Bryan et al., 2012).

Here, we describe how FORCAsT1.0 estimates deposition velocity and subsequently investigate how the choice of model formulation and parameters affect these estimates. The rate of dry deposition to the soil and foliage is calculated for all gas-phase compounds for each model layer in the canopy following the parameterisations of Wesely (1989) and Gao et al. (1993), and is described in full in Bryan et al. (2012). Deposition is assumed to occur at a rate dependent on a species-specific Henry's law coefficient, diffusivity relative to water vapor and a nominal reactivity factor accounting for enhanced uptake of some species due to reactions occurring within plant cells following uptake. Of importance here is the method of calculating the deposition velocity within the foliar layers, based on four resistances: the quasi-laminar boundary layer at the leaf surface (R_b), stomatal (R_s), mesophyll (R_m), and cuticular (R_c) resistances, such that for each trace gas (i), the deposition velocity (v_d) at each level is:

$$v_{d,i}(z) = \frac{1}{R_{b,i}(z) + R_s(z)\left(D_{\text{H}_2\text{O}} / D_i\right) + R_{m,i}(z)} + \frac{2}{R_{b,i}(z) + R_{c,i}(z)}, \tag{3}$$

where z is the height of the midpoint of the model level, and $D_{\text{H}_2\text{O}} / D_{ii}$ (=1.6 for ozone) is the ratio of the molecular diffusivities of water to the trace gas of interest (Gao et al., 1993). Resistances depend on factors such as LAI, leaf length and the reactivity factor of the trace gas and are calculated on-line in the model. Stomatal resistance, R_s, is deduced as the inverse of stomatal conductance (Ashworth et al., 2015).

The ozone deposition rate, D_r, is then calculated as:

$$D_r = v_d \times \left[\text{O}_3\right], \tag{4}$$

where $[\text{O}_3]$ is the average concentration of ozone at leaf-level in each canopy layer.

In FORCAsT1.0, stomatal conductance is calculated using the Jarvis multiplicative model. Here we extend the Jarvis approach to include photosynthesis and incorporate two coupled stomatal conductance-photosynthesis models into FORCAsT-gs, allowing the user to select between three different approaches to calculating photosynthesis and stomatal conductance (see Section 2.2). In all other respects, dry deposition remains unchanged (Ashworth et al., 2015; Bryan et al., 2012).

2.2. Physiology: Coupled Stomatal Conductance-Photosynthesis Models

There are currently three distinct approaches to modeling stomatal conductance and net photosynthesis: empirical multiplicative models that estimate stomatal conductance and thence photosynthesis rate (e.g., Jarvis, 1976); coupled stomatal conductance-photosynthesis models that simultaneously solve for both (e.g., Ball et al., 1987); and optimisation models that simultaneously maximize carbon assimilation while minimizing water loss (e.g., Medlyn et al., 2011). We describe below the key aspects of the three that we incorporated into FORCAsT-gs. A more detailed description of the mathematical formulations for each model is presented in the supplementary information.

The Jarvis model (Jarvis, 1976) assumes stomatal aperture is downregulated from a theoretical maximum by the effects of environmental conditions such as temperature, PAR, and leaf age. The scale of each down-regulation is based on experimental observations and g_s is then calculated as:

$$g_s = g_{\max} \times f_{\text{phen}} \times f_{\text{light}} \times \max\left\{f_{\min}, \left(f_{\text{temp}} \times f_{\text{VPD}} \times f_{\text{SWC}}\right)\right\}, \tag{5}$$

where g_s (mol m^{-2} s^{-1}) is stomatal conductance at each model level and $g_{\max}$ (mol m^{-2} s^{-1}) is the plant species-specific maximum value of canopy stomatal conductance for water vapor The scaling functions, f_{phen}, f_{light}, f_{temp}, f_{VPD}, and f_{SWC} have values between 0 and 1 and account for the reduction in stomatal conductance due to leaf age (phenology), photosynthetic photon flux density (PPFD, μmol m^{-2} s^{-1}; defined as the intensity of PAR reaching each square meter of the canopy per second), temperature (T, °C), vapor pressure deficit (VPD, kPa), and volumetric soil water content (SWC, m^3 m^{-3}), respectively. $f_{\min}$ is the minimum stomatal conductance during daylight. Details of the calculations of each of the functions are given in S1.1.

Net photosynthesis rate, A_n, is then assumed to be directly proportional to the conductance, g_s, such that:

$$A_n = g_s \times C_i, \tag{6}$$

where C_i is the ratio of ambient to internal concentrations of CO_2 and is normally taken as 0.7. Parameter values for each site were determined from field measurements, lab-based experiments or taken from literature for the nearest equivalent and are shown in Table S2.

The Ball-Berry coupled stomatal conductance-photosynthesis model assumes that stomatal conductance is regulated directly by the instantaneous rate of photosynthesis to balance CO_2 concentrations inside the leaf with ambient levels. Photosynthesis rate (A; μmol m^{-2} s^{-1}) at each level in the canopy is calculated following the formulations of Farquhar et al. (1980), Harley et al. (1992) and Baldocchi (1994):

$$A = V_c - 0.5 V_o - R_d, \tag{7}$$

where V_c is the carboxylation rate, V_o the oxygenation rate, R_d the dark respiration rate and

$$V_C - 0.5 V_O = \min\left[A_C, A_j\right] \times \left(1 - \Gamma / C_i\right), \tag{8}$$

that is, assuming that the photosynthesis rate is limited by either Ribulose bisphosphate saturation during carboxylation (A_c) or by the rate of electron transport for Ribulose bisphosphate regeneration during oxygenation (A_j). Γ is the CO_2 compensation point (the CO_2 concentration at which net CO_2 fixation is zero at a given O_2 level and temperature Moss et al., 1969) in the absence of dark respiration, and C_i is the intercellular CO_2 concentration (Farquhar & von Caemmerer, 1982).

The internal CO_2 concentration of the leaf, C_i is:

$$C_i = C_s - \frac{A}{g_s}, \tag{9}$$

where g_s is stomatal conductance and C_s is the CO_2 concentration at the leaf surface. Here, g_s was calculated following Ball et al. (1987) as:

$$g_s = g_o + m \frac{A * RH}{C_s}, \tag{10}$$

where g_o is the residual stomatal conductance as A tends to zero, m is a species-specific coefficient expressing the sensitivity of g_s to changes in A, and RH is the relative humidity at the leaf surface.

Medlyn et al. (2011) also assume that photosynthesis rate at each level in the canopy is the minimum of carboxylation and electron transport rate. The version incorporated into FORCAsT-gs is based on the parameterisations of Farquhar et al. (1980) for photosynthesis rate (A; μmol m^{-2} s^{-1}) in C$_3$ plants such that:

$$A = \min\left(A_j, A_c\right) - R_d, \tag{11}$$

where R_d (mol m^{-2} s^{-1}) is the leaf dark respiration.

Stomatal conductance (g_s) is then modeled following optimisation theory (Medlyn et al., 2011) in which stomatal aperture is regulated to maximize carbon gain while simultaneously minimizing water loss:

$$g_s \approx g_o + \left(1 + \frac{g_1}{\sqrt{D}}\right)\frac{A}{C_s}, \tag{12}$$

where g_o (mol m^{-2} s^{-1}) is the residual stomatal conductance as A approaches zero and g_1 is the slope of the sensitivity of g_s to changes in A. D (kPa) is the vapor pressure deficit and C_s (μmol mol^{-1}) the CO$_2$ concentration at the leaf surface as before. The values of g_o and g_1 are determined at the species or plant functional type (PFT) level from experimental data, and in this study were obtained from Lin et al. (2015) and De Kauwe et al. (2015). Values for each site are listed in Table S2.

The Jarvis model includes soil moisture stress as one of the factors limiting stomatal conductance. The relationship between SWC and g_s is modeled following Büker et al. (2015):

$$f_{\text{swc}} = \begin{cases} 1 & \text{for PAW}t \le \text{PAW} \le 1 \\ \left(1 - f_{\min}\right)\dfrac{\text{PAW}}{\text{PAW}_t} + f_{\min} & \text{for } 0 < \text{PAW} < \text{PAW}t \end{cases}, \tag{13}$$

where PAW is plant available water and is given by:

$$\text{PAW} = \frac{\theta - \theta_w}{\theta_f - \theta_w}, \tag{14}$$

where θ is the volumetric soil water content (SWC, m^3 m^{-3}), θ_f and θ_w are the SWC at field capacity and wilting point, respectively, and PAW$_t$ is a site-specific threshold of the fraction of water in the soil that is, available to the plant estimated from site soil characteristics.

For both the Ball-Berry and Medlyn models, we assumed the effect of water stress on photosynthesis to be the result of biochemical limitations as demonstrated in previous studies (e.g., see Egea et al., 2011). A soil moisture stress function (β) was therefore applied to the maximum rate of RuBP carboxylation (V_{cmax}) and the maximum rate of electron transport ($J_{\max}$) to reflect the impact of soil moisture deficit on plant gas exchange. β ranges between 1 (in the absence of water stress) and 0 (at wilting point) and is calculated based on soil water content following Porporato et al. (2001); Keenan et al. (2009, 2010):

$$\beta = \begin{cases} 1 & \text{for } \theta \ge \theta_C \\ \left[\dfrac{\left(\theta - \theta w\right)}{\left(\theta_c - \theta w\right)}\right]^q & \text{for } \theta_w < \theta < \theta_C \\ 0 & \text{for } \theta < \theta_w \end{cases}, \tag{15}$$

where θ (m^3 m^{-3}) is the volumetric soil moisture, θ_w is the wilting point (m^3 m^{-3}), and θ_c is a critical soil moisture content above which water stress is found not to affect plant-atmosphere CO$_2$ and water vapor exchange (Egea et al., 2011). Porporato et al. (2001) reported a non-linear relationship between soil moisture deficit and limitation of plant physiological processes such as stomatal conductance and photosynthesis, encapsulated here by q, a site-specific empirical factor. The nature of the impact of drought stress on different plant species and at different sites (drought tolerance) can be varied by the choice of value of q in model soil-moisture parameterisations. A more detailed derivation of q can be found in Porporato et al. (2001) and Keenan et al. (2010). In this study, q was based on observations at each site.

Photosynthesis and stomatal conductance are then estimated using the water-stressed values $V_{c\max*}$ and $J_{\max*}$:

$$V_{c\max*} = V_{c\max} \times \beta, \tag{16a}$$

$$J_{\max*} = J_{\max} \times \beta. \tag{16b}$$

The Medlyn model further assumes direct limitation to stomatal conductance due to water stress following De Kauwe et al. (2015), such that stomatal conductance becomes:

$$g_s \approx g_o + \left(1 + \frac{g_{1\beta}}{\sqrt{D}}\right)\frac{A}{C_s}. \tag{17}$$

These soil moisture stress functions are applied in all of the simulations conducted here.

2.3. FLUXNET Sites and Data

Five sites representative of the major forest biomes (tropical, temperate, and boreal) have been used in this study. An overview of each site is given below with further information provided in Table S1 and Figure S1. The sites are all included in the FLUXNET2015 data set which categorizes each location by IGBP ecosystem type (Loveland et al., 2000).

We obtained hourly and half-hourly observations of PAR, air temperature, CO_2 concentration, volumetric soil water content, wind speed and direction, relative humidity and atmospheric pressure (Pa) from the FLUXNET2015 data set. These data were used as driving data for FORCAsT simulations. The measured CO_2 from net ecosystem exchange (NEE) is partitioned into GPP and ecosystem respiration (Reco) using model parameterizations based on nighttime or daytime fluxes (Lasslop et al., 2010; Reichstein et al., 2005). We use GPP estimated from nighttime fluxes (GPP_NT_VUT_REF) for model evaluation as this is a standard benchmarking protocol in the land surface modeling community (see e.g., Harper et al., 2021; Otu-Larbi, Conte, et al., 2020). In this study, GPP is assumed to be zero in the absence of light. The methodology for estimating GPP and gap-filling of meteorological variables via Marginal Distribution Sampling (MDS) are fully described in Pastorello et al. (2020).

Ozone concentration data were obtained for IT-Cp2, FI-Hyy, and US-Blo but are not readily available for US-Ha1 or BR-Sa1 for the periods considered in this study (Table S1). For these sites we used reanalysis data from the Copernicus Atmospheric Monitoring Service (CAMS; https://atmosphere.copernicus.eu) which have been shown to reproduce observed tropospheric ozone to within 10% (see e.g., Inness et al., 2013; Wagner et al., 2021).

2.3.1. Santarém-Km67-Primary Forest (BR-Sa1)

BR-Sa1 is in Amazonian Brazil and consists of primary forest comprising a wide range of tree species of varied ages, epiphytes, and high numbers of decaying logs. A flux tower, which was established in 2000 for the Large-scale Biosphere-Atmosphere (LBA) experiment (Rice et al., 2004) is sited on a large level plateau with forest cover stretching 5–40 km in all directions (Goulden et al., 2004). There is closed-canopy forest to an average height of 40 m within the footprint of the flux tower, with numerous emergent trees up to 55 m in height (Rice et al., 2004).

Figure 1 shows volumetric soil moisture and meteorological data from BR-Sa1 (yellow line) for an average annual profile. The site is categorized as Tropical Evergreen Forest and has a hot humid tropical environment with average rainfall of 1,920 mm y^{-1} and annual average temperature of ~25°C, with little diurnal or seasonal variability (Rice et al., 2004).

The clay soil has little organic content and retains water well. Soil moisture is not routinely measured at BR-Sa1 and we use data from a nearby site (BR-Sa3 at the 83 km marker) located in the same area of forest. A selective logging experiment commenced at BR-Sa3 shortly after the main LBA campaign and has continued to this day. Less than 5% of aboveground biomass is removed each time, leaving only small gaps between areas of closed-canopy forest (Goulden et al., 2004). Soil moisture at 5 cm depth at BR-Sa3 responds quickly to precipitation, ranging between ~0.30 and 0.47 m^3 m^{-3}. At a depth of 250 cm, there is little variation with
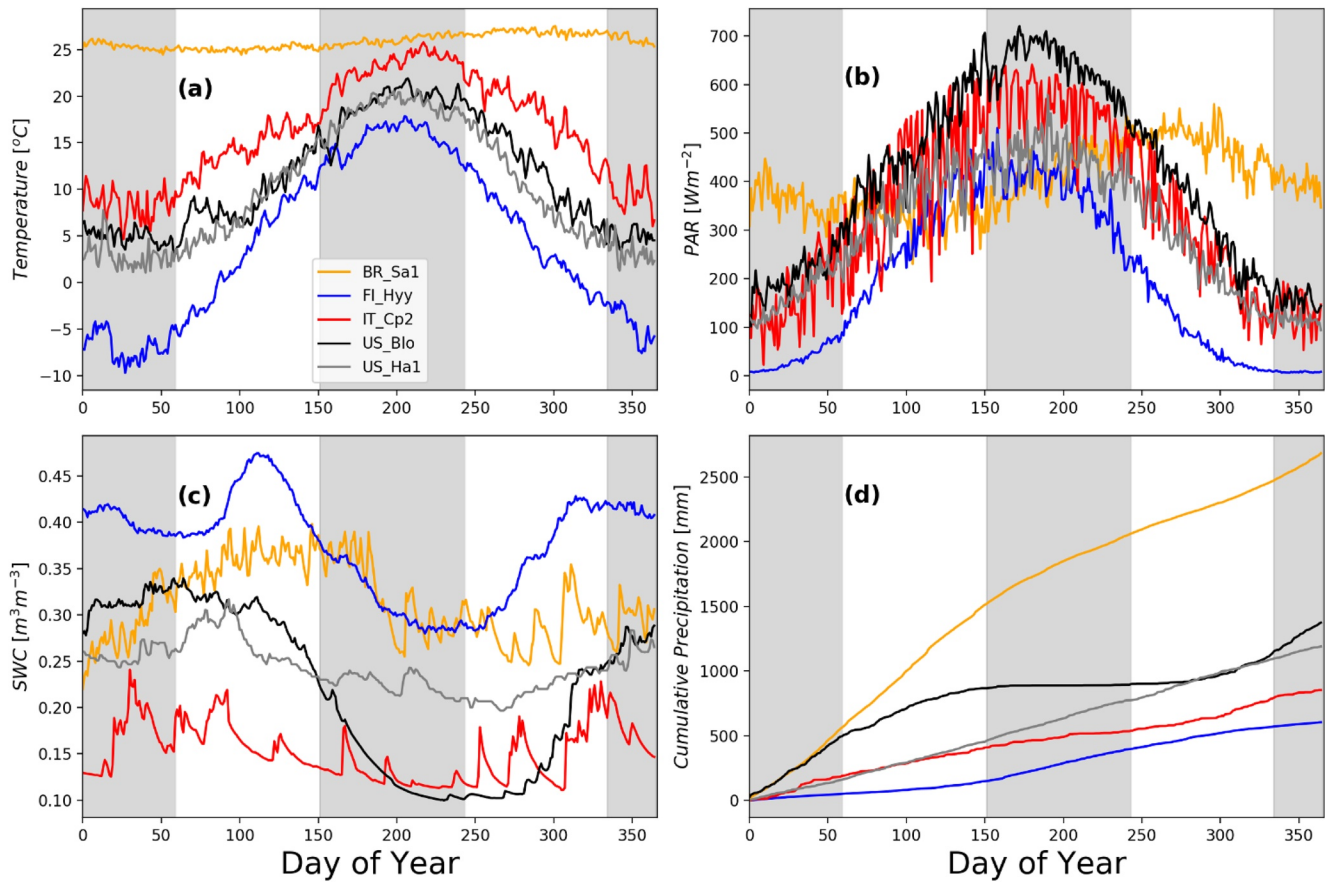
Figure 1. Site conditions and meteorology showing (a) soil moisture (volumetric soil water content (SWC); m^3 m^{-3}); (b) cumulative precipitation (mm); (c) 2-m air temperature (ºC) and (d) photosynthetically active radiation (PAR) at the top of the canopy (W m^{-2}) for an average year at BR-Sa1 (yellow), FI-Hyy (blue), IT-Cp2 (red), US-Blo (black), and US-Ha1 (gray).

soil moisture relatively constant at ~0.46 m^3 m^{-3} during the wet season, declining gradually to ~0.42 m^3 m^{-3} by the end of the dry season (Rice et al., 2004).

2.3.2. Hyytiälä (FI-Hyy)

FI-Hyy is located in the sub-boreal climate zone at the SMEAR II (Station for Measuring Ecosystem-Atmosphere Relation) boreal forest research station at Hyytiälä, ~220 km NW of Helsinki (Hari & Kulmala, 2005; Rinne et al., 2007). The 73-m flux tower is situated on relatively level ground, surrounded by predominantly uniform age (~60-year-old) Scots pine (*Pinus sylvestris*) with an average canopy height of 14 m (Hari & Kulmala, 2005; Suni et al., 2003).

Figure 1 shows volumetric soil moisture and meteorological data from FI-Hyy (blue line) for an average year. The site is categorized as Boreal Evergreen Forest with climatological (1959–2014) average annual temperature of 3.5°C and precipitation of 693 mm y^{-1} falling predominantly as snow during the winter months (SMEARII, 2021; Suni et al., 2003). Average monthly temperatures range between −7.7°C in February, and 16°C in July (SMEARII, 2021). Prevailing winds are SSW and are generally moderate, with average annual windspeed of ~2.8 m s^{-1} and maximum of 14 m s^{-1} (SMEARII, 2021). The soil comprises sandy and coarse silty glacial till (Suni et al., 2003). Soil moisture peaks at >0.45 m^3 m^{-3} after snow melt and drops to ~0.30 m^3 m^{-3} or lower during occasional summer droughts.

2.3.3. Castelporziano (IT-Cp2)

IT-Cp2 is located at Grotta di Piastra within the Presidential Estate at Castelporziano, on the Thyrrenian coast ~25 km SW of Rome. The 6,000 ha Estate has been used for environmental research since 1951 with

a flux tower first installed in 1996. The current tower is ~20 m tall and surrounded almost exclusively by even-aged Holm oak (*Quercus ilex*) of average ~14 m height (Fares et al., 2019). This is a typical macchia species, well-adapted to an environment characterized by hot dry summers and nutrient poor sandy soils (Fares et al., 2009).

Figure 1 shows volumetric soil moisture and meteorological data from IT-Cp2 (red line) for an average year. The site is categorized as Temperate Evergreen Forest and has a Mediterranean environment with an average rainfall of 745 mm y^{-1} of which <100 mm y^{-1} falls in the summer months (May–early September). Between 1996 and 2011, mean monthly temperatures ranged between 8.4 and 24.7°C, with a maximum temperature of 30.3°C and minimum of 5.0°C recorded in August and February respectively (Fusaro et al., 2015).

The soil is sandy and freely draining. Soil moisture is thus highly variable and tightly coupled to precipitation events. Soil moisture averaged over a depth of 10–50 cm ranges from ~5% at the end of the summer drought period to ~32% during the winter (Fares et al., 2019).

2.3.4. Blodgett Forest (US-Blo)

US-Blo is located in a uniform-age Ponderosa pine plantation in the Sierra Nevada mountain range on the western coast of the continental USA. The plantation was established in 1990 and a 15-m flux tower, which has been the site of long-term monitoring and numerous intensive field campaigns, erected in 1997 (Goldstein et al., 2000). The average height of the canopy is ~9 m (Park et al., 2014).

Figure 1 shows volumetric soil moisture and meteorological data from US-Blo (black line) for an average year. The site is categorized as Temperate Evergreen Forest with a Mediterranean climate. Annual average precipitation is ~1,630 mm y^{-1} with little rain during the summer months (May–early September). Average daily temperatures range between 17-24°C in the summer, and 0–9°C in the winter (Goldstein et al., 2000).

The soil is predominantly free draining loam, and soil moisture tracks precipitation (Goldstein et al., 2000). Average soil moisture at a depth of 10–20 cm ranges from ~0.10 m^3 m^{-3} during summer droughts to just below 0.35 m^3 m^{-3} in the winter.

2.3.5. Harvard Forest (US-Ha1)

US-Ha1 is located within a ~1,600 ha area of old-growth (75+ years) mixed forest in NE USA that has been the site of long-term ecological and environmental monitoring since 1,907. A 30-m flux tower was erected in 1990 and has been used for continuous measurements and summer field campaigns since (Goldstein et al., 1998; McKinney et al., 2011). The average height of the canopy is ~24 m (Clifton et al., 2019).

Figure 1 shows volumetric soil moisture and meteorological data from US-Ha1 (gray line) for an average year. The site is categorized as Temperate Deciduous Forest with the footprint of the tower dominated by red oak (*Quercus rubra*) and red maple (*Acer rubrum*), although there are a number of red and white pines (*Pinus resinosa* and *P. strobus*) to the NW of the tower (Clifton et al., 2019). Annual average precipitation is ~1,000 mm y^{-1} and is relatively evenly distributed through the year. Average daily temperatures range between ~20 °C in the summer and ~1°C in the winter. The soil around the flux tower is a sandy loam (Allen, 1995). Soil moisture typically ranges from ~0.25 to 0.55 m^3 g^{-3}, but can drop below 0.20 m^3 m^{-3} during (infrequent) drought years (Clifton et al., 2019).

2.4. Simulations

LAI can be estimated by FORCAsT-gs but here we use in-situ or remote sensing observations. Forests are classified as evergreen if at least 80% of the trees maintain their leaves throughout the year (Sasaki et al., 2016). Thus, we use fixed LAI values obtained from site measurements for for BR-Sa1, IT-Cp2, FI-Hyy, and US-Blo. For the temperate deciduous forest (US-Ha1) we use in-situ observations.

Stomatal conductance, photosynthesis rate (instantaneous fluxes of CO_2) and deposition velocity are calculated for each leaf angle class (9 sunlit and 1 shaded) for each foliage-containing level within the canopy in FORCAsT-gs using each of the three physiological approaches outlined in Section 2.2. These are then

weighted by leaf angle fraction and leaf area distribution at each level and summed over all model layers to obtain canopy-scale conductance, photosynthesis rates (canopy-top fluxes of CO_2) and deposition velocity.

During preliminary model configuration at each site, site-specific phenological and canopy structure were set to best fit modeled to observed GPP. However, the physiological parameters used in each of the three coupled stomatal conductance-photosynthesis algorithms were set to average values reported from previous studies in-situ at similar ecosystems or in controlled environments. These semi-optimized configurations provided our baseline simulations at each site (hereafter referred to as BASE).

To determine the sensitivity of the model to perturbations in the physiological parameters, which are mostly derived from controlled environment experiments, and to provide uncertainty bounds for our estimates of GPP and ozone deposition rates, we conducted a series of sensitivity tests. Only parameters with a direct relationship to stomatal conductance were used in these sensitivity tests to ensure consistency in approach.

In the Jarvis multiplicative model, average values of g_{max} for specific plant functional types are typically used, but Hoshika et al. (2018) found variations of up to 70% between the upper and lower bounds of g_{max} and the mean for different PFTs. Here, we use the mean values for different forest ecosystems for baseline simulations (JV) and the upper and lower bounds as JV+ and JV−, respectively (Table S3).

For the Ball-Berry coupled stomatal conductance-photosynthesis model, the coefficient m (Equation 10) describing the relationship between stomatal conductance and photosynthesis typically ranges between 9 and 12. We use these as our lower (BB−) and upper (BB+) bounds, with the baseline (BB) set to a value of 10. See Table S3 for further details of parameter settings.

The equivalent coefficient, g_1 (Equation 12), is tested in the Medlyn optimisation model. We take the upper (MD+) and lower (MD−) bounds of g_1 as reported by De Kauwe et al. (2015) and Lin et al. (2015) for different forest ecosystems with error margins of 2%–10%. Our baseline simulations (MD) use the average value for each site. Further details of parameter settings are given in Table S3.

At the end of the simulation period, average annual and diel profiles of total canopy photosynthesis were calculated and compared with observed GPP. To assess the relative performance of each model at each of the five sites, we define a single summary statistic that encompasses the three key model performance indicators for temporal trends (correlation), absolute values (cRMSE) and variability (normSD) in a single value. As all three elements are important in evaluating overall model skill, we use a simple combination assigning the same weight to each. This summary statistic is calculated as:

$$\text{Summary} = \text{cRMSE} \times \left(1.0 - r^2\right) \times \left|\text{normSD} - 1.0\right|, \tag{18}$$

where r^2 is the coefficient of determination, normSD is the normalised standard deviation and cRMSE is the centered root mean square error. The closer this value is to zero, the closer the model fits the observations.

3. Results

3.1. BASE

We first evaluate the skill of each of the three stomatal conductance-photosynthesis models to reproduce the average diel and annual profiles of GPP at each site for the time periods shown in Table S1. The BASE simulations presented here use the parameter values given in Table S2.

As shown by the orange lines on Figure 2, the multiplicative stomatal conductance model (JV) reproduces the seasonal variation in GPP at all sites except for BR-Sa1, although it substantially overestimates seasonal GPP at the three broadleaf forests (BR-Sa1, IT-Cp2, and US-Ha1) and underestimates at the Boreal needleleaf forest (FI-Hyy). At BR-Sa1, JV overestimates GPP by a factor of 1.5–2. At IT-Cp2 and US-Ha1, however, while JV overestimates GPP by 50%–100% in spring and summer it performs well in the rest of the year. For FI-Hyy, JV consistently underestimates productivity from summer through to early autumn, by a factor of 2. However, the model reproduces GPP at US-Blo, which is also a needleleaf forest, to within 20% of the observations at all times of the year. This suggests that the phenology of Boreal ecosystems is not well-captured.
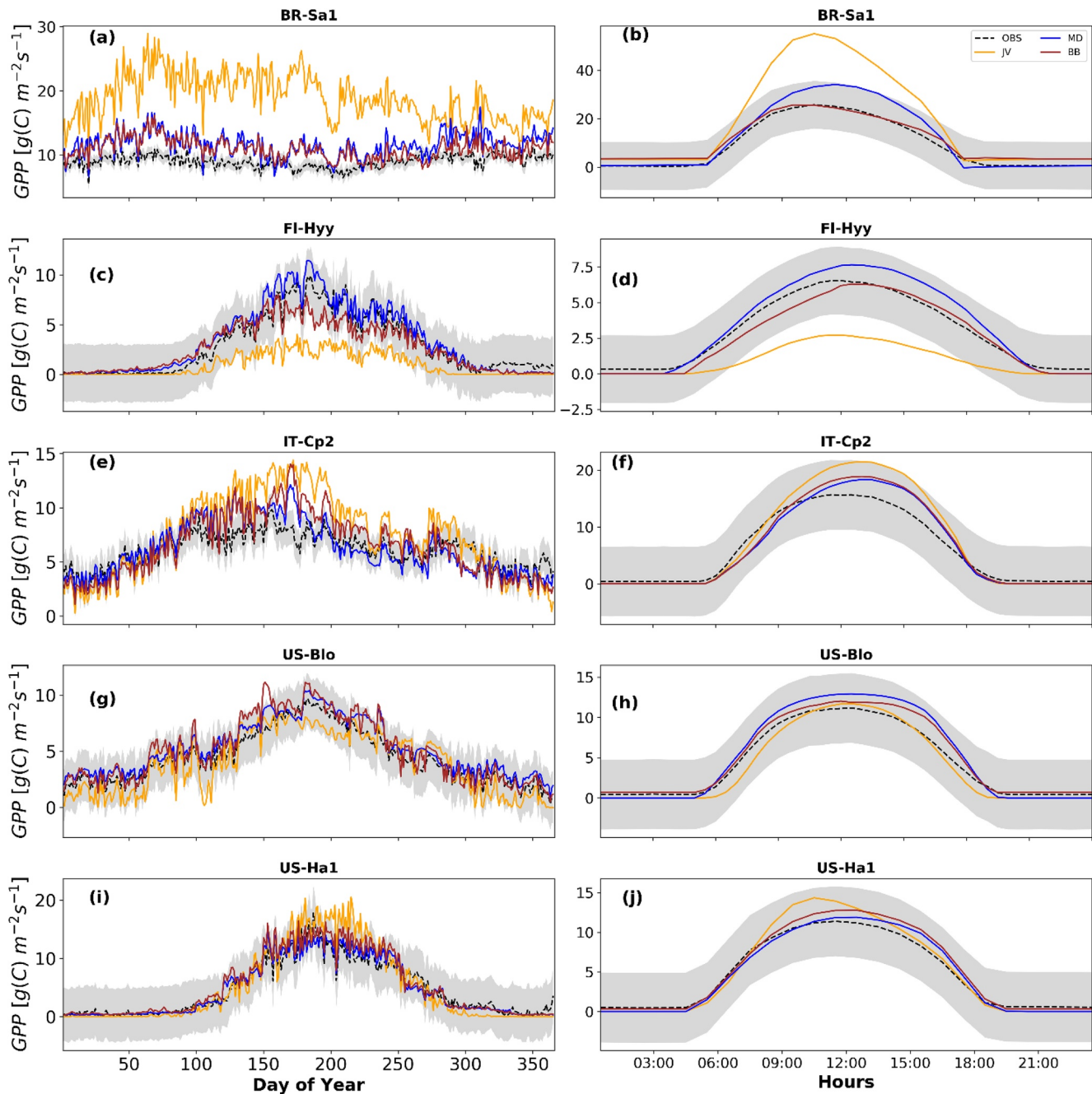
Figure 2. Net photosynthesis for an average year at each of the five FLUXNET sites, from top to bottom row: BR-Sa1, FI-Hyy, IT-Cp2, US-Blo, and US-Ha1. The left column shows average annual and the right average diel profiles of gross primary productivity (GPP, a measure of photosynthesis rate) estimated from the Jarvis multiplicative (gold), Ball-Berry coupled (red) and Medlyn stomatal optimisation coupled (blue) stomatal conductance-photosynthesis models. The black dashed lines show observed GPP, with gray shaded areas indicating ± one standard deviation from the daily average GPP.

The diel profiles of modeled GPP using JV follow a similar inter-site pattern to that of the seasonal profile with overestimation of diurnal GPP at BR-SA1, IT-Cp2, and US-Ha1 by 5%–200%, and underestimation of ~75% at FI-Hyy. The coupled stomatal conductance-photosynthesis model (BB) reproduces the observed seasonality and magnitude of GPP within 10%–50% at all but the tropical BR-Sa1 ecosystem as shown by the brown lines on the first column of Figure 2. BB underestimates summer GPP at FI-Hyy by 30% but overestimates GPP at IT-Cp2 by a similar margin in the summer when seasonal drought occurs. It closely matches observed GPP throughout the season at US-Blo and US-Ha1 with <10% variation between model

estimates and observations. Although BB overestimates GPP by as much as 50% at BR-Sa1 throughout the year, it outperforms both JV and MD at this site.

The diurnal profile of GPP estimated by BB confirms its superior performance at the tropical site BR-Sa1, with modeled GPP closely matching the observations during the day. The diurnal profile at the other sites shows that BB underestimates GPP by ∼5% in the early hours of the day at FI-Hyy and IT-Cp2 but tends to overestimate GPP by ∼20% in the later afternoon. Output from the Medlyn model (MD) is shown in blue in Figure 2. While MD follows the seasonal fluctuation of GPP at BR-Sa1, estimated fluxes are a factor of ∼1.5 higher than observations throughout the year. This overestimation of GPP at the tropical site is also apparent in the profile over the course of an average day. By contrast, at the two Mediterranean sites, MD reproduces both the observed seasonal and diurnal profile of GPP and is within 20% of the observed values at any time during the year or day. MD also shows excellent agreement with both the magnitude and timing of observed GPP throughout the year at FI-Hyy but overestimates the average diurnal profile of GPP by ∼20%. MD performs best at the temperate deciduous forest site, US-Ha1, where there is <5% between model estimates and observations across both the year and day.

The superior performance of MD across sites is confirmed by the Taylor diagrams in Figure 3 and the summary statistics in Table S4. MD exhibits high correlation (0.56–0.98), and low deviation (1.01–1.92) and error (0.90–3.03). Summary statistics ranging between 0.0003 and 1.25 confirm it as the best performing model overall. As shown by the summary statistic in Table S4, which ranges between 0.01 and 0.99, BB outperforms JV at all sites. As summarized by the Taylor diagram in Figure 3, BB's performance is better than that of JV, with cRMSE of 1.07–2.47, r^2 of 0.85–0.97 (excluding BR-Sa1) and normSD of 0.80–1.82. The summary statistics for JV range from 0.02 at US-Blo where JV performs well at reproducing observed GPP to 28.86 at BR-Sa1 where it overestimates both seasonal and diurnal profile of GPP. Seasonal cRMSE ranging between 1.24-10.64, normSD between 0.40-3.72 and r^2 as low as 0.01 at BR-Sa1, further confirms the relatively poor performance of JV. These results show that MD provides the best estimates of GPP at four of the five forest sites used in this study (FI-Hyy, IT-Cp2, US-Blo, and US-Ha1) while BB was the overall best performer at BR-Sa1. JV was the least skilful of the three models, substantially overestimating GPP at BR-Sa1, IT-Cp2, and US-Ha1, and underestimating at FI-Hyy. All three models were most successful in reproducing observed GPP at the temperate deciduous forest, US-Ha1, and poorest at the tropical forest, BR-Sa1.

### 3.2. Sensitivity of Stomatal Conductance to Model Parameters

The BASE simulations used mid-range values for species-specific parameters g_{max} (JV; Equation 5), m (BB; Equation 10), and g_1 (MD; Equation 12). As described in Section 2.4, we carried out sensitivity tests using lower and upper bound estimates for these parameters. Here we analyze the effect that these parameter changes have on estimated photosynthesis rates for each of the three models, identifying similarities and differences in responses between sites and providing an estimate of uncertainty bounds for GPP and stomatal conductance in each case.

3.2.1. JV

The plant species-specific theoretical maximum value of canopy stomatal conductance for water vapor (g_{max}; Equation 5) is central to the performance of the JV model in reproducing observed plant gas exchange. Changes in g_{max} lead to proportional changes in both stomatal conductance (Figure S4) and GPP (Figure 4) at all sites. In general, decreasing g_{max} to its lower limit causes up to a factor of 2 reduction in GPP depending on the site, while an increase to the upper bound increases GPP by similar magnitudes.

At the tropical and temperate forests (BR-Sa1, IT-Cp2, US-Blo, and US-Ha1) where JV over-estimates GPP, using instead the lower limit of g_{max} (JV−) provides the best model-observation fit in both seasonal and diel cycles at BR-Sa1, but substantially underestimates GPP at IT-Cp2, US-Blo and US-Ha1.

By contrast, at FI-Hyy, where JV underestimates GPP, the use of the upper bound of g_{max} (JV+) reduced, but does not completely overcome, model underestimation through the seasons or over the course of an average day. JV+ modeled GPP was around half to two-thirds of observed fluxes, a substantial improvement on the factor of 2 underestimations in JV.
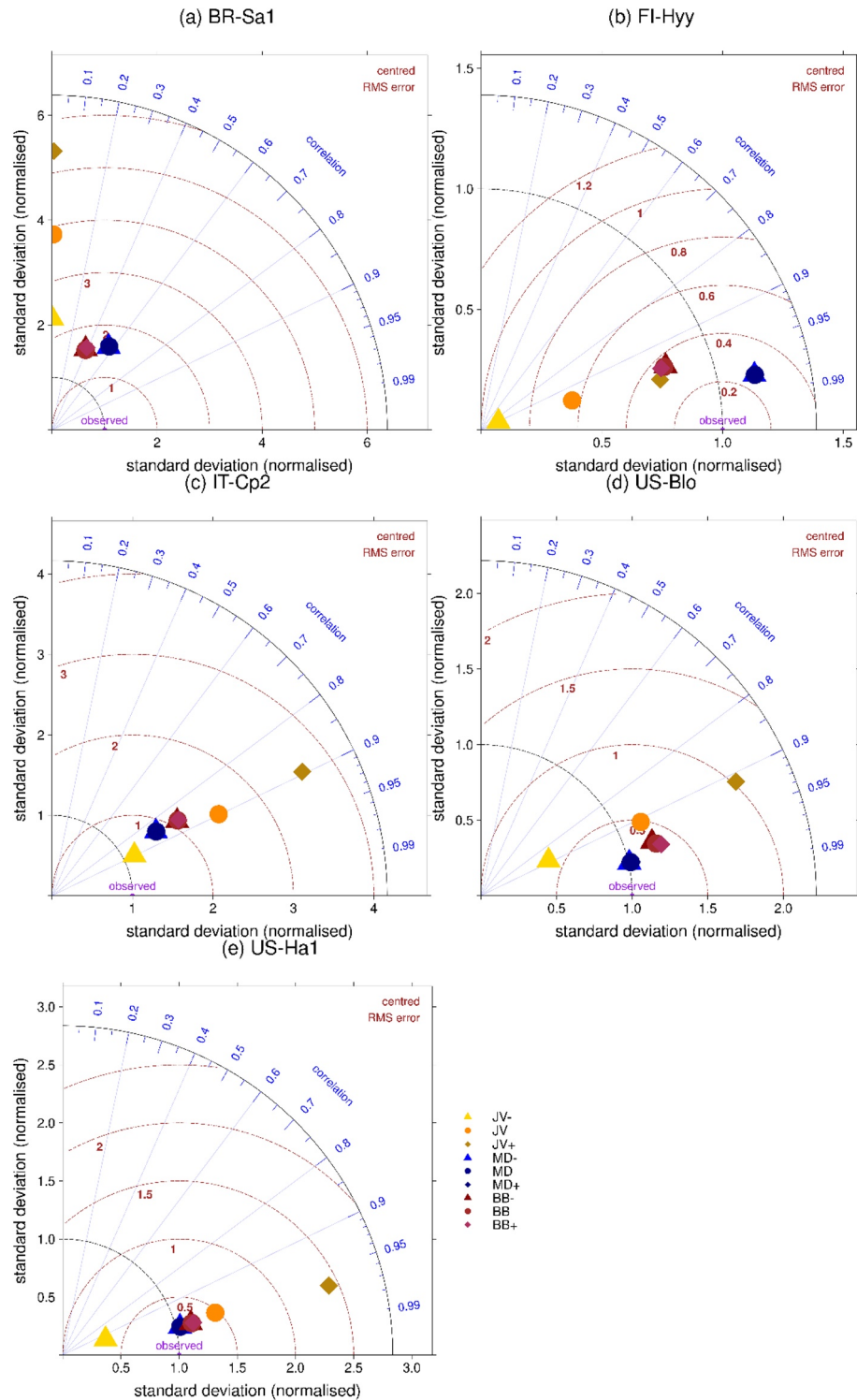
Figure 3. Taylor Diagram summarizing model output statistics from FORCAsT sensitivity tests. Observed GPP has SD = 1.0, RMSE = 0.0, and r = 1.0 (purple circle). Black and brown dashed curves and blue lines show normalised standard deviation (SD), centered root mean squared error (RMSE) and correlation coefficients (r) respectively against observations for each model on each diagram. The summary statistics for each JV simulation are shown by gold symbols, BB by red, MD simulation by blue. BASE simulations are denoted by circles, lower bounds (TEST−) by triangles, and upper bounds (TEST+) by diamonds. Note that JV, MD, and BB in these plots are the BASE simulations described in Sections 2.5.1 and 3.1, and Figure 2.
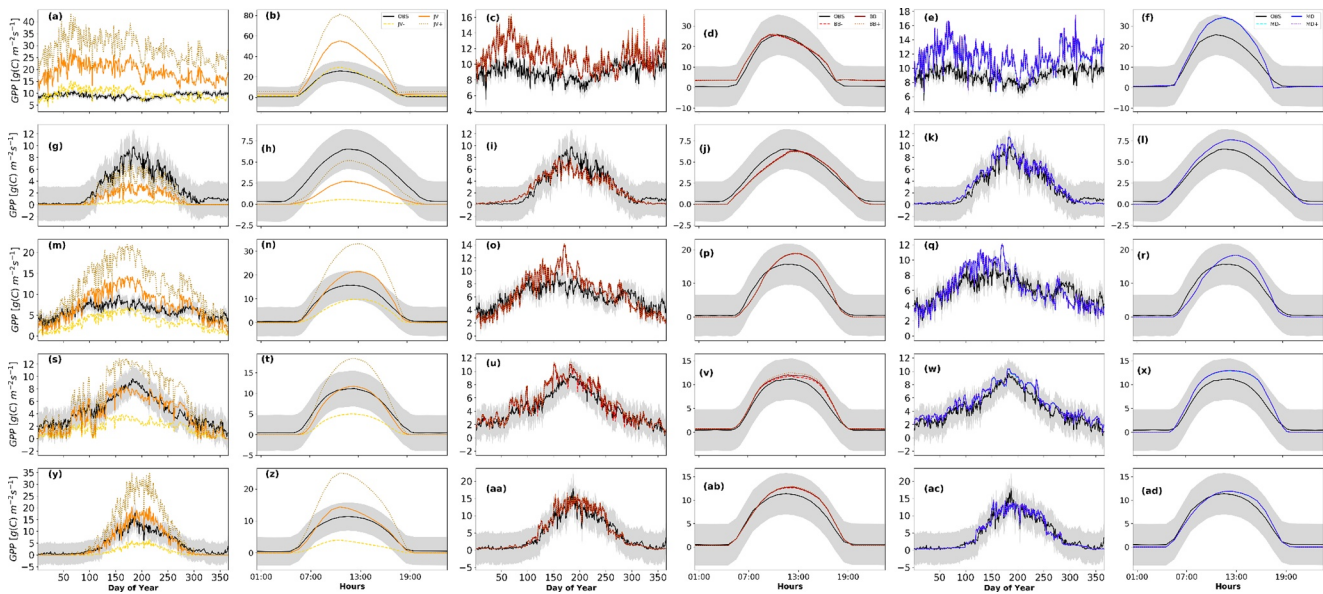
Figure 4. Modeled and observed GPP for an average year at, from top to bottom: BR-Sa1, FI-Hyy, IT-Cp2, US-Blo, and US-Ha1. Columns 1 and 2 (gold) areJarvis (), columns 3 and 4 (red) Ball-Berry, and columns 5 and 6 (blue) Medlyn. Solid lines denote the unperturbed (BASE) simulation as shown in Figure 2 for each model, with dashed paler line for TEST− and dashed darker line for TEST+ simulations, respectively. The black lines show observed GPP at each site with gray shaded areas indicating ± one standard deviation from daily and hourly average GPP.

As shown by the Taylor plots presented in Figure 3, and Table S4, both normalised SD and centered RMSE are substantially increased in JV−. While this is a major improvement in overall model performance at BR-Sa1 (with cRMSE reduced from 10.6 in JV to 2.36 in JV−), JV− substantially worsens model fit at all the other sites. JV+ exacerbates the tendency to overestimate across all sites, with summary statistics increasing to 0.22–87.40. The correlation coefficient between modeled and measured GPP is unchanged as it essentially summarizes the temporal fit.

3.2.2. BB

For the BB parameterization, stomatal conductance and net photosynthesis rate are explicitly linked and solved simultaneously. Variations in species-specific response parameters therefore directly affect both g_s and GPP. Similarly to JV, the upper bound increases and lower bound reduces flux estimates compared to the baseline.

In BB, increasing m, that is, the change in photosynthesis rate for a given change in stomatal conductance, results in proportionally larger increases in GPP than the decreases resulting from reducing m. GPP is slightly over-estimated by BB at all sites (except during the summer months at FI-Hyy where modeled fluxes are lower than observed). BB- therefore provides a better fit to observed GPP across all sites except FI-Hyy where BB+ performs better. It should be noted however, that changes in GPP (0.5%–1.0%) are considerably smaller than those observed for JV between the upper and lower bound simulations.

This is further corroborated by the Taylor diagrams (Figure 3) summarizing the average, upper and lower bound simulations. Across all sites, there is little change in correlation between estimated and observed GPP, reflecting the minor changes in temporal profile. NormSD also remains virtually unchanged between simulations for GPP fluxes (~1.0 at US-Blo and US-Ha1, ~0.8 at FI-Hyy and ~2.0 at IT-Cp2). cRMSE is consistently low for all simulations at the extra-tropical sites (~1.0–1.2 for GPP at US-Blo and FI-Hyy, and 1.4–1.8 at IT-Cp2 and US-Ha1), indicating the relatively good match to absolute values. By contrast, cRMSE remains high (>2.5) at the tropical rainforest site, BR-Sa1, where a high normSD and low correlation coefficient also confirm the poor performance of the model at capturing both the magnitude and temporal variations in GPP at this ecosystem. The BASE simulation of BB provides the closest fit to observed GPP at BR-Sa1.

3.2.3. MD

Similarly to BB, changes in g_1 in MD result in very small changes in estimated GPP. At the two Mediterranean sites (IT-Cp2 and US-Blo) where GPP is overestimated in the baseline (MD) simulations, MD-provides a closer fit to observations (Figure 3) although the change is only ~1%. Changes in g_1 have a negligible effect on GPP at BR-Sa1, FI-Hyy or US-Ha1 (Figure 3), where droughts are rare and there is less need for plants to conserve water, that is, where there is less conflict between maximizing photosynthesis and minimizing transpiration.

As shown in the Taylor diagrams (Figure 3), increasing the value of g_1 from the average to the upper bound improves the correlation between estimated and observed GPP at US-Blo, while decreasing the value improves the fit slightly at IT-Cp2. As suggested by the temporal profiles, there is no noticeable change in correlation at BR-Sa1, FI-Hyy or US-Ha1. The normSD for GPP are very close to 1.0 (i.e., a perfect fit to observations) and centered RMSE <0.5 at FI-Hyy, US-Ha1 and US-Blo but near 2.0 and 1.0, respectively at IT-Cp2, again likely a result of the severity of droughts at Castelporziano, where water conservation is a key driver of stomatal conductance. All three statistics remain poor at BR-Sa1, where r^2 remains virtually unchanged at ~0.6, normSD at 2.0, and cRMSE at ~1.8 for all values of g_1. Considering the relatively small changes observed in GPP in response to changes in g_1, we conclude that the mean values of g_1 are sufficient for estimating stomatal conductance and GPP using the Medlyn model at these sites.

3.2.4. Summary of Sensitivity Tests

As shown in Figures 3 and 4, and Table S4, GPP estimates in JV were more sensitive to variations in g_{max} than BB and MD estimates were to m and g_1, respectively. However, modeled GPP does not vary by the same magnitude as the variation in model parameters. For instance, modeled GPP values in JV− and JV differ from BASE (JV) estimates by as much as 100% in response to up to 60% variation in g_{max} causing substantial differences in model output statistics (Figure 3 and Table S4). GPP estimates using upper and lower bounds of m (BB) and g_1 (MD) only differ by 1%–5% in response to a 10%–20% change in the model parameterization. It must be noted that these sensitivity tests only focus on stomatal conductance parameters in all three models. Tests conducted on photosynthetic parameters such as V_{cmax} and J_{max} have shown a greater difference in estimated GPP compared to what we find here (e.g., see Fares et al., 2019) but do not have an equivalent in JV.
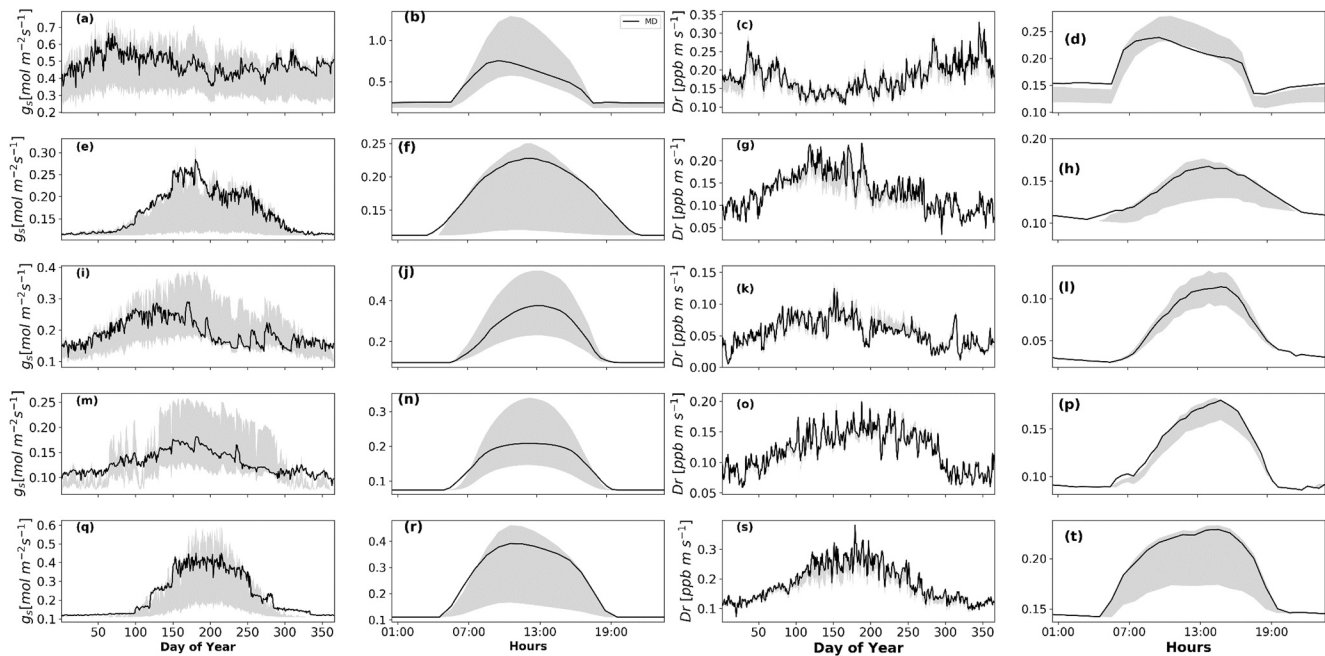
3.3. Stomatal Conductance

As the three physiology models in FORCAsT-gs explicitly couple photosynthesis and stomatal conductance, we now assume that the parameterization that best represents GPP (as a proxy for photosynthesis) at each of the sites also best captures fluctuations in stomatal aperture. Figure 5 presents the performance of the models at each site relative to the stomatal conductance or ozone deposition rate simulated by the best-performing model.

The first and second columns of Figure 5 shows the average seasonal and diurnal profiles of stomatal conductance at each site with that estimated by the best performing model shown as a black line (i.e., assumed as "truth"). The gray shading indicates the full range of stomatal conductance estimated by the various model configurations.

At the tropical site, BR-Sa1, the BB model, which best captures GPP, is taken to represent observed stomatal conductance. Stomatal conductance estimated with the model that has the lowest GPP estimates (JV−) is ~75% lower while the configuration with the greatest overestimation of GPP (JV+) is ~25% higher. The difference between the models remains almost constant throughout the year at this tropical site. The divergences in stomatal conductance at FI-Hyy, IT-Cp2, US-Blo, and US-Ha1 are seasonal. For these sites, MD-is used to represent observed g_s due to its lower summary statistics shown in Table S4. The difference between the models that over or underestimate GPP is <30% in the winter and spring and increases rapidly to >100% at IT-Cp2 and US-Blo in the summer, and >200% at FI-Hyy and US-Ha1.

The diel profile of stomatal conductance between the best and worst performing models is similar to the seasonal profile observed at each site. As shown by the second columns of Figure 5, BR-Sa1, IT-Cp2, and US-Blo show the widest variation in modeled stomatal conductance between the different model configurations

Figure 5. Stomatal conductance (columns 1 and 2) and ozone deposition rates (columns 3 and 4) for an average year and day at each of the five FLUXNET sites, from top to bottom: BR-Sa1, FI-Hyy, IT-Cp2, US-Blo, and US-Ha1. Solid lines black lines denote the output from the model that best reproduced gross primary productivity (GPP) at each site as shown in Figures 3 and 4. The shaded regions indicate the spread in stomatal conductance and deposition rates across all the model sensitivity tests.

during peak periods of the day. There is about 10% overestimation of peak daytime stomatal conductance values at FI-Hyy and US-Ha1 between the best and overestimating model configurations. On the contrary, the models that underestimate GPP at these sites (JV−) also underestimate stomatal conductance by and >50%.

3.4. Ozone Deposition

The differences in simulated stomatal conductance between configurations of FORCAsT-gs affect estimated ozone deposition velocity and hence the rate at which ozone is lost to this key sink. Figure S6 shows the seasonal and diel profiles of variations in ozone deposition velocity between the models. The tropical site, BR-Sa1, and the temperate broadleaf forest, US-Ha1, have the highest estimated ozone deposition velocities as expected from their higher g_s compared to the other sites. This higher gs and hence ozone deposition velocities are likely due to the fact that plants in these forests also have bigger leaf sizes and higher leaf area index–highlighting the role of forest structure and characteristics in plant physiological processes (Meyers & Baldocchi, 1988; Padro, 1996).

The deposition velocity is however dependent on several resistances as shown in Equation 3, including the stomatal resistance (the inverse of g_s). As a result, the models that overestimate GPP and g_s do not necessarily overestimate seasonal deposition velocity when compared to the best performing model across all sites. However, the model configurations that underestimate GPP and g_s also underestimate seasonal ozone deposition velocity, although to a lesser extent. For example, JV- underestimates GPP and g_s by a factor of two during the peak growing season but only underestimates deposition velocity by ∼15%, with an average value of 0.36 cm s^{-1} compared with 0.42 cm s^{-1} estimated with the best performing model (MD). Similarly, at the tropical site, the average deposition velocity in the optimal model configuration (BB) is 0.88 cm s^{-1}. These deposition velocity estimates are similar to those found in other studies for similar ecosystems and PFTs (e.g., Hardacre et al., 2015; Silva & Heald, 2018). This value is 13% higher than the average deposition velocity in JV− which underestimates GPP and 6% lower than that of JV+ which overestimates GPP.

The variation between modeled deposition velocities at FI-Hyy, IT-Cp2, and US-Blo between the model configurations is similar to those described for BR-Sa1 and US-Ha1 although the absolute values are smaller. The only exception here is at IT-Cp2 where JV+ overestimates deposition velocity in the summer just as it did for GPP and g_s. The model divergence in diel profile of ozone deposition velocity exhibits similar variability to that of the seasonal profile.

The seasonal changes in deposition velocity are also very different to that of g_s at their respective sites. Ozone deposition velocities at BR-Sa1, IT-Cp2, and US-Ha1, show the greatest variations, ranging between <5% and ~30% for model configurations that over or underestimate GPP respectively, relative to the model configuration that produces the best summary statistics for each site, as defined by Equation 18 and summarized in Table S4. The two needleleaf forests, FI-Hyy and US-Blo show the least variation in seasonal deposition velocities of <10%.

As shown in Equation 4, ozone deposition rates depend on ozone concentration as well as deposition velocity. Hence, while the differences estimated in deposition velocity would be expected to produce changes in ozone deposition rates at the study sites, they will not be directly proportional.

Figure S7 shows the average ozone concentrations for each study site for the relevant simulation periods. As ozone is produced through photochemical processes concentrations at all sites peak during the spring and summer and decline steadily in the autumn and winter.

Figures 5, S8 and S9 shows that the seasonal variation in ozone deposition rate closely follows the seasonal variation in ozone concentration at all sites. On the contrary, the diel profile of ozone deposition differs from that of the concentration. While ozone concentrations at all sites peak in the late afternoon or early evening, deposition rates are highest just after midday when g_s and deposition velocity are at a maximum. This clearly indicates that deposition velocity, and hence stomatal conductance, is the key determinant of deposition rates on shorter timescales, while atmospheric ozone concentrations drive longer temporal trends. The greatest variations in seasonal and diurnal deposition rates between different model configurations, indicated by the gray shaded areas on Figure 5, are observed at FI-Hyy and US-Ha1, as for the deposition velocities.

The diel profile of ozone deposition rates, and their variations due to changes in stomatal conductance parameterisations, are similar to those of the deposition velocities (Figure S6). Variations in deposition rates estimated by JV+ which overestimates GPP and stomatal conductance, and the best-fit models averaged 0.10%–10% across sites. Figures S8 and S9 show that ozone deposition rates estimated with JV are more sensitive to changes in model parameters with variations of up to 20% observed between different JV configurations. MD and BB ozone deposition rates are less sensitive to model parameters with variations of less than 5% observed between BASE simulations and those using and upper and lower limits of g_1 and m (Figure S8).

The seasonal variations observed in deposition rates are much lower than the variations in either stomatal conductance or deposition velocity across all sites. There is only ~1% variation between seasonal ozone deposition rates in model configurations which overestimate GPP and the best performing model across sites, apart from IT-Cp2 where deposition rate varies by ~5% in the summer. Seasonal deposition rates estimated by model configurations with the lowest GPP are 7%–13% lower than those estimated with the best performing model configurations (Figure 5). By contrast, modeled stomatal conductance and deposition velocities vary by up to 100% and up to 30% respectively for these same model configurations (Figure 5), confirming the modulating effect of ozone concentrations.

The role of ozone concentrations in determining ozone deposition rates is exemplified at BR-Sa1. Average g_s and deposition velocity are a factor of two higher at this site than US-Ha1 which has the next highest values. However, the average ozone deposition rates at BR-Sa1 are approximately the same as those at US-Ha1 (0.18 ppb cms^{-1}). This is due to lower average ozone concentrations at BR-Sa1 (20 ppb) compared to US-Ha1 (43 ppb).

4. Discussion and Conclusion

We have found that ozone deposition rates estimated using stomatal conductance simulated by two of the most widely used stomatal conductance-photosynthesis models can vary by as much as 10% depending on ecosystem, season and time of day. As dry deposition is the primary sink for tropospheric ozone, this has potentially significant implications for estimated ozone budgets across space and time. Stomatal conductance and GPP estimated using the Jarvis multiplicative model appear particularly sensitive to choice of model parameters whereas estimates made using Ball-Berry and Medlyn coupled stomatal conductance-photosynthesis models exhibit less variability.

By introducing the Jarvis, Ball-Berry and Medlyn parameterisations of stomatal conductance and photosynthesis into FORCAsT1.0, a 1-D column model of trace gas exchange between a forest canopy and the atmosphere (Ashworth et al., 2015; Otu-Larbi, Bolas, et al., 2020; Otu-Larbi, Conte, et al., 2020), we were able to evaluate the performance of the three physiological models via comparison of simulated photosynthesis with long-term measurements of GPP taken from the FLUXNET2015 data set (Pastorello et al., 2020). We find that all three models reproduce the seasonal and diel variations in GPP well at a range of forest types, Boreal evergreen (FI-Hyy), Temperate deciduous (US-Ha1), and Mediterranean evergreen (IT-Cp2 and US-Blo), but struggle to capture seasonality at a Tropical broadleaf evergreen site (BR-Sa1).

As shown in Figures 2 and 4, the Medlyn stomatal optimisation model provides the best overall performance at four of the five FLUXNET sites used in this study (FI-Hyy, IT-Cp2, US-Blo, and US-Ha1), with estimates of GPP within 20%, but is out-performed by the Ball-Berry coupled stomatal conductance-photosynthesis model at BR-Sa1. The superior performance of MD compared to BB at could be expected as MD was specifically developed as an improvement on BB to optimize carbon gain while limiting water loss (Medlyn et al., 2011). Except for US-Blo, where JV reproduces the observed annual and diel profiles of GPP to within 20%, the Jarvis multiplicative model either substantially overestimates or underestimates GPP by as much as a factor of two. The relatively poor performance of JV in reproducing observed GPP is perhaps not surprising since photosynthesis estimates are based on a simple assumption of a linear relationship between stomatal conductance and carbon assimilation (Equation 6).

The superior performance of the Medlyn optimisation model in the two Mediterranean climates could also be due to the fact that vegetation response to soil moisture stress is better accounted for through a combination of stomatal and biochemical limitations (e.g., see De Kauwe et al., 2015; Lin et al., 2015; Otu-Larbi, Conte, et al., 2020). BB, by comparison, assumes that drought stress directly downregulates photosynthesis rates or is the result of biochemical limitation only (e.g., see Best et al., 2011; Clark et al., 2011; Fares et al., 2019). This finding is supported by previous work which shows that the choice of drought stress parameterization is an important factor that determines model performance in a water stressed environment (Egea et al., 2011; Keenan et al., 2010).

The poor performance of the models at the tropical evergreen site (BR-Sa1) is likely due to the assumption of a uniform forest structure for this evergreen forest site throughout the year. Subsequently, f_{phen} in JV (Equation 5) is set to a value of 1 and constant LAI is used in estimating photosynthetic capacity in BB and MD models. A modeling study by Flack-Prain et al. (2019) indicates that changes in LAI could account for up to 33% of observed variations in Amazonian forest GPP. This suggests the need for an improved understanding of changes in forest structure and phenology in tropical ecosystems to obtain more accurate model estimation of GPP at this and other tropical sites (Rödig et al., 2018). In addition, photosynthetic rates and stomatal conductance are controlled by solar radiation and temperature and limited by stress factors like drought and air pollutants including ozone (Nemani et al., 2003). For BR-Sa1, both temperature and PAR (Figures 1a and 1b; orange lines) remain fairly constant throughout the year which would lead to higher modeled photosynthetic capacity in BB and MD since modeled V_{cmax} and J_{max} are reliant on temperature. Seasonal variations in V_{cmax} and J_{max} are reported to be a major source of uncertainty in GPP estimates in Amazonian forests (Flack-Prain et al., 2019). It is worth noting that US-Blo and IT-Cp2 which are also evergreen forest, are treated similarly, but as shown in Figures 2 and 4, the models perform better at these sites, perhaps due to a compensating error in modeling drought stress.

Results from sensitivity tests conducted on key stomatal conductance parameters in JV, BB, and MD models reveal that modeled GPP and stomatal conductance values are highly sensitive to the choice of conductance

parameters. Variations of ~5%–75% from base model estimates are observed in modeled GPP and stomatal conductance in response to ~10%–60% variation in model parameters. Such wide differences could reduce the reliability of estimated reductions in crop or plant productivity due to air pollutants such as ozone.

The findings from this study make it imperative that more measurements of these key conductance parameters are made to improve understanding and model representation of dry deposition. The Jarvis model shows greater sensitivity to choice of parameter values than either Ball-Berry or Medlyn. It must be noted that the Jarvis parameter g_{max} is typically measured in sunlit leaves at the top of the canopy. Leaves below the canopy often differ in their shape and leaf angle from those at the top of the canopy (Niinemets, 2010). The JV model as implemented in FORCAsT and elsewhere assumes the same g_{max} for all angle classes and model levels. More work is needed to improve the parameterization of variations in g_{max} for different levels in the canopy and leaf angle classes.

We conclude that the Medlyn coupled stomatal conductance-photosynthesis model would be the best default selection. However, our model simulations also point to the need for improved stomatal conductance-photosynthesis model parameterisations for tropical ecosystems where seasonality is driven by contrasts in precipitation rather than temperature and solar radiation.

We tested the response of ozone deposition rate in different ecosystems to changes in stomatal conductance parameterization while keeping model calculation of other resistances unchanged. The choice of stomatal conductance model parameters is found to be a very important factor in determining ozone deposition rates across all sites. Seasonal and daily deposition rates to the forest canopy change by as much as 13% with implications for air quality modeling and assessment of ozone damage to crops and plants. Most models used in assessing air quality at global, regional, and local levels consider dry deposition using variants of the same Wesely deposition scheme used in FORCAsT-gs (Hardacre et al., 2015). Many international assessments of ozone damage to crops and forests are based on dose-response parameters developed using the JV model (e.g., see Buker et al., 2015; Emberson et al., 2000, Hayes et al., 2007; Mills et al., 2011). Like air quality models, dose-response relationships rely on ozone deposition rates and their accuracy and reliability could be severely diminished if the appropriate model parameterisations are not used. Large uncertainty in modeled deposition rates due to the choice of model parameters, as found in this study, could therefore affect modeled surface ozone concentrations with negative implications for air quality monitoring as well as assessments of plant productivity losses from ozone damage. This is especially true for models that rely on the Jarvis multiplicative model to estimate stomatal conductance. Our results highlight the need to carefully consider the choice of model parameters as this will ultimately determine model performance.

Similar to other studies, we find higher stomatal conductance and ozone deposition velocities at tropical and broadleaf forest site compared to needleleaf and coniferous forests (e.g., see Emberson et al., 2001; Fowler et al., 2001, 2011; Kumar et al., 2011; Silva & Heald, 2018). The larger LAI at the broadleaf forests (BR-Sa1 and US-Ha1) leads to greater canopy conductance, lower stomatal resistance, and subsequently higher deposition velocity as these are important for estimating total canopy and leaf boundary resistance (Meyers & Baldocchi, 1988; Padro, 1996). Ozone deposition velocities at BR-Sa1 are up to a factor of three higher than those at IT-Cp2, US-Blo, and FI-Hyy. However, the difference in ozone deposition rates are much lower (<30%) due to lower ozone concentrations at this remote forest site.

Our findings of the sensitivity of stomatal conductance estimates to parameter and algorithm choice could also have important implications in modeling biogenic volatile organic compound (BVOC) emissions. Current BVOC emission models rely on leaf temperature and solar radiation to drive emission rates and are known to reproduce observations for a range of forest ecosystems and climates within a factor of two (e.g., see Guenther et al., 1993, 1995; 2006). However, such models have been shown to struggle to reproduce diurnal emission patterns of short-chained carboxylic acids and aldehydes, leading to suggestions that the failure to include stomatal conductance in such models could be a limiting factor in model performance (Kesselmeier et al., 1997; Martin et al., 1999; Niinemets & Reichstein, 2003; Staudt et al., 2000). Including stomatal control of emission rates in land-atmosphere models would need to account for the sensitivity of simulated stomatal conductance to the choice of physiological model.

Conflict of Interests

The authors declare no conflicts of interest relevant to this study.

Data Availability Statement

FLUXNET2015 data for BR-Sa1, FI-Hyy, IT-Cp2, US-Blo, and US-Ha1 are available from https://fluxnet.fluxdata.org/data/fluxnet2015-dataset/. A user account is required. The doi of each data set is provided in Table S1. FORCAsT-gs is available for download on request to the corresponding author.

References

Ainsworth, E. A., Yendrek, C. R., Sitch, S., Collins, W. J., & Emberson, L. D. (2012). The effects of tropospheric O3 on net primary productivity and implications for climate change. *Annual Review of Plant Biology*, *63*, 637–661. https://doi.org/10.1146/annurev-arplant-042110-103829

Allen, A. (1995). Soil science and survey at Harvard Forest. *Soil Survey Horizons*, *36*(4), 133–142. https://doi.org/10.2136/sh1995.4.0133

Ashworth, K., Chung, S. H., Griffin, R. J., Chen, J., Forkel, R., Bryan, A. M., & Steiner, A. L. (2015). FORest Canopy Atmosphere Transfer (FORCAsT) 1.0: A 1-D model of biosphere–atmosphere chemical exchange. *Geoscientific Model Development*, *8*(11), 3765–3784. https://doi.org/10.5194/gmd-8-3765-2015

Avnery, S., Mauzerall, D. L., Liu, J., & Horowitz, L. W. (2011). Global crop yield reductions due to surface ozone exposure: 1. Year 2000 crop production losses and economic damage. *Atmospheric Environment*, *45*(13), 2284–2296. https://doi.org/10.1016/j.atmosenv.2010.11.045

Baldocchi, D. (1988). A multi-layer model for estimating sulfur dioxide deposition to a deciduous oak forest canopy. *Atmospheric Environment*, *22*, 869–884. https://doi.org/10.1016/0004-6981(88)90264-8

Baldocchi, D. (1994). An analytical solution for coupled leaf photosynthesis and stomatal conductance models. *Tree Physiology*, *14*(7–8–9), 1069–1079. https://doi.org/10.1093/treephys/14.7-8-9.1069

Ball, J. T., Woodrow, I. E., & Berry, J. A. (1987). A model predicting stomatal conductance and its contribution to the control of photosynthesis under different environmental conditions. In: *Progress in photosynthesis research* (pp. 221–224). Springer. https://doi.org/10.1007/978-94-017-0519-6_48

Best, M. J., Pryor, M., Clark, D. B., Rooney, G. G., Essery, R., Ménard, C. B., et al. (2011). The joint UK land environment simulator (JULES), model description–Part 1: Energy and water fluxes. *Geoscientific Model Development*, *4*(3), 677–699. https://doi.org/10.5194/gmd-4-677-2011

Blackadar, A. K. (1962). The vertical distribution of wind and turbulent exchange in a neutral atmosphere. *Journal of Geophysical Research*, *67*(8), 3095–3102. https://doi.org/10.1029/JZ067i008p03095

Bryan, A. M., Bertman, S. B., Carroll, M. A., Dusanter, S., Edwards, G. D., Forkel, R., et al. (2012). In-canopy gas-phase chemistry during CABINEX 2009: Sensitivity of a 1-D canopy model to vertical mixing and isoprene chemistry. *Atmospheric Chemistry and Physics*, *12*(18), 8829–8849. https://doi.org/10.5194/acp-12-8829-2012

Bryan, A. M., Cheng, S. J., Ashworth, K., Guenther, A. B., Hardiman, B. S., Bohrer, G., & Steiner, A. L. (2015). Forest-atmosphere BVOC exchange in diverse and structurally complex canopies: 1-D modeling of a mid-successional forest in northern Michigan. *Atmospheric Environment*, *120*, 217–226. https://doi.org/10.1016/j.atmosenv.2015.08.094

Büker, P., Feng, Z., Uddling, J., Briolat, A., Alonso, R., Braun, S., et al. (2015). New flux based dose–response relationships for ozone for European forest tree species. *Environmental Pollution*, *206*, 163–174. https://doi.org/10.1016/j.envpol.2015.06.033

Chen, J., Mao, H., Talbot, R. W., & Griffin, R. J. (2006). Application of the CACM and MPMPO modules using the CMAQ model for the eastern United States. *Journal of Geophysical Research*, *111*(D23), D23S25. https://doi.org/10.1029/2006JD007603

Clark, D. B., Mercado, L. M., Sitch, S., Jones, C. D., Gedney, N., Best, M. J., et al. (2011). The joint UK land environment simulator (JULES), model description – Part 2: Carbon fluxes and vegetation dynamics. *Geoscientific Model Development*, *4*(3), 701–722. https://doi.org/10.5194/gmd-4-701-2011

Clifton, O. E., Fiore, A. M., Munger, J. W., & Wehr, R. (2019). Spatiotemporal controls on observed daytime ozone deposition velocity over northeastern US forests during summer. *Journal of Geophysical Research: Atmospheres*, *124*(10), 5612–5628. https://doi.org/10.1029/2018JD029073

Cowan, I. R., & Farquhar, G. D. (1977). *Stomatal function in relation to leaf metabolism and environment.*

Damour, G., Simonneau, T., Cochard, H., & Urban, L. (2010). An overview of models of stomatal conductance at the leaf level. *Plant, Cell and Environment*, *33*(9), 1419. https://doi.org/10.1111/j.1365-3040.2010.02181.x

De Kauwe, M. G., Kala, J., Lin, Y. S., Pitman, A. J., Medlyn, B. E., Duursma, R. A., et al. (2015). A test of an optimal stomatal conductance scheme within the CABLE land surface model. *Geoscientific Model Development*, *8*(2), 431–452. https://doi.org/10.5194/gmd-8-431-2015

Egea, G., Verhoef, A., & Vidale, P. L. (2011). Towards an improved and more flexible representation of water stress in coupled photosynthesis–stomatal conductance models. *Agricultural and Forest Meteorology*, *151*(10), 1370–1384. https://doi.org/10.1016/j.agrformet.2011.05.019

Emberson, L. D., Ashmore, M. R., Cambridge, H. M., Simpson, D., & Tuovinen, J. P. (2000). Modelling stomatal ozone flux across Europe. *Environmental Pollution*, *109*(3), 403–413. https://doi.org/10.1016/S0269-7491(00)00043-9

Emberson, L. D., Ashmore, M. R., Simpson, D., Tuovinen, J. P., & Cambridge, H. M. (2001). Modelling and mapping ozone deposition in Europe. *Water, Air, and Soil Pollution*, *130*(1), 577–582. https://doi.org/10.1023/A:1013851116524

Fares, S., Alivernini, A., Conte, A., & Maggi, F. (2019). O3 and particle fluxes in a Mediterranean forest predicted by the AIRTREE model. *The Science of the Total Environment*, *682*, 494–504. https://doi.org/10.1016/j.scitotenv.2019.05.109

Fares, S., Mereu, S., Scarascia Mugnozza, G., Vitale, M., Manes, F., Frattoni, M., et al. (2009). The ACCENT-VOCBAS field campaign on biosphere-atmosphere interactions in a Mediterranean ecosystem of Castelporziano (Rome): Site characteristics, climatic and meteorological conditions, and eco-physiology of vegetation. *Biogeosciences*, *6*(6), 1043–1058. https://doi.org/10.5194/bg-6-1043-2009

Farquhar, G. D., & Von Caemmerer, S. (1982). Modelling of photosynthetic response to environmental conditions. In: *Physiological plant ecology II* (pp. 549–587). Springer. https://doi.org/10.1007/978-3-642-68150-9_17

Farquhar, G. D., von Caemmerer, S. V., & Berry, J. A. (1980). A biochemical model of photosynthetic CO_2 assimilation in leaves of C_3 species. *Planta*, *149*(1), 78–90. https://doi.org/10.1007/BF00386231

Flack-Prain, S., Meir, P., Malhi, Y., Smallman, T. L., & Williams, M. (2019). The importance of physiological, structural and trait responses to drought stress in driving spatial and temporal variation in GPP across Amazon forests. *Biogeosciences*, *16*(22), 4463–4484. https://doi.org/10.5194/bg-16-4463-2019

Forkel, R., Klemm, O., Graus, M., Rappenglück, B., Stockwell, W. R., Grabmer, W., et al. (2006). Trace gas exchange and gas phase chemistry in a Norway spruce forest: A study with a coupled 1-dimensional canopy atmospheric chemistry emission model. *Atmospheric Environment*, *40*, 28–42. https://doi.org/10.1016/j.atmosenv.2005.11.070

Fowler, D., Flechard, C., Cape, J. N., Storeton-West, R. L., & Coyle, M. (2001). Measurements of ozone deposition to vegetation quantifying the flux, the stomatal and non-stomatal components. *Water, Air, and Soil Pollution*, *130*(1), 63–74. https://doi.org/10.1023/A:1012243317471

Fowler, D., Nemitz, E., Misztal, P., Di Marco, C., Skiba, U., Ryder, J., et al. (2011). Effects of land use on surface–atmosphere exchanges of trace gases and energy in Borneo: Comparing fluxes over oil palm plantations and a rainforest. *Philosophical Transactions of the Royal Society B: Biological Sciences*, *366*(1582), 3196–3209. https://doi.org/10.1098/rstb.2011.0055

Franks, P. J., Berry, J. A., Lombardozzi, D. L., & Bonan, G. B. (2017). Stomatal function across temporal and spatial scales: Deep-time trends, land-atmosphere coupling and global models. *Plant Physiology*, *174*(2), 583–602. https://doi.org/10.1104/pp.17.00287

Franks, P. J., Bonan, G. B., Berry, J. A., Lombardozzi, D. L., Holbrook, N. M., Herold, N., & Oleson, K. W. (2018). Comparing optimal and empirical stomatal conductance models for application in Earth system models. *Global Change Biology*, *24*(12), 5708–5723. https://doi.org/10.1111/gcb.14445

Fusaro, L., Salvatori, E., Mereu, S., Silli, V., Bernardini, A., Tinelli, A., & Manes, F. (2015). Researches in Castelporziano test site: Ecophysiological studies on Mediterranean vegetation in a changing environment. *Rendiconti Lincei*, *26*(3), 473–481. https://doi.org/10.1007/s12210-014-0374-1

Gao, W., Wesely, M. L., & Doskey, P. V. (1993). Numerical modeling of the turbulent diffusion and chemistry of NOx, O_3, isoprene, and other reactive trace gases in and above a forest canopy. *Journal of Geophysical Research*, *98*(D10), 18339–18353. https://doi.org/10.1029/93JD01862

Geiger, H., Barnes, I., Bejan, I., Benter, T., & Spittler, M. (2003). The tropospheric degradation of isoprene: An updated module for the regional atmospheric chemistry mechanism. *Atmospheric Environment*, *37*(11), 1503–1519. https://doi.org/10.1016/S1352-2310(02)01047-6

Goldstein, A. H., Goulden, M. L., Munger, J. W., Wofsy, S. C., & Geron, C. D. (1998). Seasonal course of isoprene emissions from a midlatitude deciduous forest. *Journal of Geophysical Research*, *103*(D23), 31045–31056. https://doi.org/10.1029/98JD02708

Goldstein, A. H., Hultman, N. E., Fracheboud, J. M., Bauer, M. R., Panek, J. A., Xu, M., et al. (2000). Effects of climate variability on the carbon dioxide, water, and sensible heat fluxes above a ponderosa pine plantation in the Sierra Nevada (CA). *Agricultural and Forest Meteorology*, *101*(2–3), 113–129. https://doi.org/10.1016/S0168-1923(99)00168-9

Goulden, M. L., Miller, S. D., Da Rocha, H. R., Menton, M. C., de Freitas, H. C., e Silva Figueira, A. M., & de Sousa, C. A. D. (2004). Diel and seasonal patterns of tropical forest CO_2 exchange. *Ecological Applications*, *14*(sp4), 42–54. https://doi.org/10.1890/02-6008

Griffin, R. J., Dabdub, D., & Seinfeld, J. H. (2005). Development and initial evaluation of a dynamic species-resolved model for gas phase chemistry and size-resolved gas/particle partitioning associated with secondary organic aerosol formation. *Journal of Geophysical Research*, *110*(D5). https://doi.org/10.1029/2004JD005219

Griffin, R. J., Nguyen, K., Dabdub, D., & Seinfeld, J. H. (2003). A coupled hydrophobic-hydrophilic model for predicting secondary organic aerosol formation. *Journal of Atmospheric Chemistry*, *44*(2), 171–190. https://doi.org/10.1023/A:1022436813699

Guenther, A., Hewitt, C. N., Erickson, D., Fall, R., Geron, C., Graedel, T., et al. (1995). A global model of natural volatile organic compound emissions. *Journal of Geophysical Research*, *100*(D5), 8873–8892. https://doi.org/10.1029/94JD02950

Guenther, A., Karl, T., Harley, P., Wiedinmyer, C., Palmer, P. I., & Geron, C. (2006). Estimates of global terrestrial isoprene emissions using MEGAN (model of emissions of gases and aerosols from nature). *Atmospheric Chemistry and Physics*, *6*(11), 3181–3210. https://doi.org/10.5194/acp-6-3181-2006

Guenther, A., Zimmerman, P. R., Harley, P. C., Monson, R. K., & Fall, R. (1993). Isoprene and monoterpene emission rate variability: Model evaluations and sensitivity analyses. *Journal of Geophysical Research*, *98*(D7), 12609. https://doi.org/10.1029/93JD00527

Hardacre, C., Wild, O., & Emberson, L. (2015). An evaluation of ozone dry deposition in global scale chemistry climate models. *Atmospheric Chemistry and Physics*, *15*(11), 6419–6436. https://doi.org/10.5194/acp-15-6419-2015

Hari, P., & Kulmala, M. (2005). Station for measuring ecosystem atmosphere relations (SMEAR II). *Boreal Environmental Research*, *10*, 315–322.

Harley, P. C., Thomas, R. B., Reynolds, J. F., & Strain, B. R. (1992). Modelling photosynthesis of cotton grown in elevated CO_2. *Plant, Cell and Environment*, *15*(3), 271–282. https://doi.org/10.1111/j.1365-3040.1992.tb00974.x

Harper, A. B., Williams, K. E., McGuire, P. C., Duran Rojas, M. C., Hemming, D., Verhoef, A., et al. (2021). Improvement of modeling plant responses to low soil moisture in JULESvn4. 9 and evaluation against flux tower measurements. *Geoscientific Model Development*, *14*(6), 3269–3294. https://doi.org/10.5194/gmd-14-3269-2021

Hayes, F., Mills, G., Harmens, H., & Norris, D. (2007). *Evidence of widespread ozone damage to vegetation in Europe (1990-2006)*. ICP Vegetation Programme Coordination Centre.

Hetherington, A. M., & Woodward, F. I. (2003). The role of stomata in sensing and driving environmental change. *Nature*, *424*(6951), 901–908. https://doi.org/10.1038/nature01843

Hoshika, Y., Osada, Y., De Marco, A., Penuelas, J., & Paoletti, E. (2018). Global diurnal and nocturnal parameters of stomatal conductance in woody plants and major crops. *Global Ecology and Biogeography*, *27*(2), 257–275. https://doi.org/10.1111/geb.12681

Inness, A., Baier, F., Benedetti, A., Bouarar, I., Chabrillat, S., Clark, H., et al. (2013). The MACC reanalysis: An 8 yr data set of atmospheric composition. *Atmospheric Chemistry and Physics*, *13*(8), 4073–4109. https://doi.org/10.5194/acp-13-4073-2013

Jarvis, P. G. (1976). The interpretation of the variations in leaf water potential and stomatal conductance found in canopies in the field. *Philosophical Transactions of the Royal Society of London B Biological Sciences*, *273*(927), 593–610. https://doi.org/10.1098/rstb.1976.0035

Keenan, T., García, R., Friend, A. D., Zaehle, S., Gracia, C., & Sabate, S. (2009). Improved understanding of drought controls on seasonal variation in Mediterranean forest canopy CO_2 and water fluxes through combined in situ measurements and ecosystem modelling. *Biogeosciences*, *6*(8), 1423–1444. https://doi.org/10.5194/bg-6-1423-2009

Keenan, T., Sabate, S., & Gracia, C. (2010). Soil water stress and coupled photosynthesis–conductance models: Bridging the gap between conflicting reports on the relative roles of stomatal, mesophyll conductance and biochemical limitations to photosynthesis. *Agricultural and Forest Meteorology*, *150*(3), 443–453. https://doi.org/10.1016/j.agrformet.2010.01.008

Kesselmeier, J., Bode, K., Hofmann, U., Müller, H., Schäfer, L., Wolf, A., et al. (1997). Emission of short chained organic acids, aldehydes and monoterpenes from Quercus ilex L. and Pinus pinea L. in relation to physiological activities, carbon budget and emission algorithms. *Atmospheric Environment*, *31*, 119–133. https://doi.org/10.1016/S1352-2310(97)00079-4

Kumar, A., Chen, F., Niyogi, D., Alfieri, J. G., Ek, M., & Mitchell, K. (2011). Evaluation of a photosynthesis-based canopy resistance formulation in the Noah land-surface model. *Boundary-Layer Meteorology*, *138*(2), 263–284. https://doi.org/10.1007/s10546-010-9559-z

Lasslop, G., Reichstein, M., Detto, M., Richardson, A. D., & Baldocchi, D. D. (2010). Comment on Vickers et al. Self-correlation between assimilation and respiration resulting from flux partitioning of eddy-covariance CO_2 fluxes. *Agricultural and Forest Meteorology*, *150*(2), 312–314. https://doi.org/10.1016/j.agrformet.2009.11.003

Lin, Y. S., Medlyn, B. E., Duursma, R. A., Prentice, I. C., Wang, H., Baig, S., et al. (2015). Optimal stomatal behaviour around the world. *Nature Climate Change*, *5*(5), 459–464. https://doi.org/10.1038/nclimate2550

Loveland, T. R., Reed, B. C., Brown, J. F., Ohlen, D. O., Zhu, Z., Yang, L. W. M. J., & Merchant, J. W. (2000). Development of a global land cover characteristics database and IGBP DISCover from 1 km AVHRR data. *International Journal of Remote Sensing*, *21*(6–7), 1303–1330. https://doi.org/10.1080/014311600210191

Martin, R. S., Villanueva, I., Zhang, J., & Popp, C. J. (1999). Nonmethane hydrocarbon, monocarboxylic acid, and low molecular weight aldehyde and ketone emissions from vegetation in central New Mexico. *Environmental science & technology*, *33*(13), 2186–2192. https://doi.org/10.1021/es980468q

McKinney, K. A., Lee, B. H., Vasta, A., Pho, T. V., & Munger, J. W. (2011). Emissions of isoprenoids and oxygenated biogenic volatile organic compounds from a New England mixed forest. *Atmospheric Chemistry and Physics*, *11*(10), 4807–4831. https://doi.org/10.5194/acp-11-4807-2011

Medlyn, B. E., Duursma, R. A., Eamus, D., Ellsworth, D. S., Prentice, I. C., Barton, C. V., et al. (2011). Reconciling the optimal and empirical approaches to modelling stomatal conductance. *Global Change Biology*, *17*(6), 2134–2144. https://doi.org/10.1111/j.1365-2486.2010.02375.x

Meyers, T. P., & Baldocchi, D. D. (1988). A comparison of models for deriving dry deposition fluxes of O_3 and SO_2 to a forest canopy. *Tellus B: Chemical and Physical Meteorology*, *40*(4), 270–284. https://doi.org/10.3402/tellusb.v40i4.15916

Mills, G., Pleijel, H., Braun, S., Büker, P., Bermejo, V., Calvo, E., et al. (2011). New stomatal flux-based critical levels for ozone effects on vegetation. *Atmospheric Environment*, *45*(28), 5064–5068. https://doi.org/10.1016/j.atmosenv.2011.06.009

Moss, D. N., Krenzer, E. G., & Brun, W. A. (1969). Carbon dioxide compensation points in related plant species. *Science*, *164*(3876), 187–188. https://doi.org/10.1126/science.164.3876.187

Nemani, R. R., Keeling, C. D., Hashimoto, H., Jolly, W. M., Piper, S. C., Tucker, C. J., & Running, S. W. (2003). Climate-driven increases in global terrestrial net primary production from 1982 to 1999. *Science*, *300*(5625), 1560–1563. https://doi.org/10.1126/science.1082750s

Niinemets, Ü. (2010). Mild versus severe stress and BVOCs: Thresholds, priming and consequences. *Trends in Plant Science*, *15*(3), 145–153. https://doi.org/10.1016/j.tplants.2009.11.008

Niinemets, Ü., & Reichstein, M. (2003). Controls on the emission of plant volatiles through stomata: Differential sensitivity of emission rates to stomatal closure explained. *Journal of Geophysical Research*, *108*(D7). https://doi.org/10.1029/2002JD002626

Oliver, R. J., Mercado, L. M., Sitch, S., Simpson, D., Medlyn, B. E., Lin, Y. S., & Folberth, G. A. (2018). Large but decreasing effect of ozone on the European carbon sink. *Biogeosciences*, *15*(13), 4245–4269. https://doi.org/10.5194/bg-15-4245-2018

Otu-Larbi, F., Bolas, C. G., Ferracci, V., Staniaszek, Z., Jones, R. L., Malhi, Y., et al. (2020a). Modelling the effect of the 2018 summer heatwave and drought on isoprene emissions in a UK woodland. *Global Change Biology*, *26*(4), 2320–2335. https://doi.org/10.1111/gcb.14963

Otu-Larbi, F., Conte, A., Fares, S., Wild, O., & Ashworth, K. (2020b). Current and future impacts of drought and ozone stress on Northern Hemisphere forests. *Global Change Biology*, *26*(11), 6218–6234. https://doi.org/10.1111/gcb.15339

Padro, J. (1996). Summary of ozone dry deposition velocity measurements and model estimates over vineyard, cotton, grass and deciduous forest in summer. *Atmospheric Environment*, *30*(13), 2363–2369. https://doi.org/10.1016/1352-2310(95)00352-5

Park, J. H., Fares, S., Weber, R., & Goldstein, A. H. (2014). Biogenic volatile organic compound emissions during BEARPEX 2009 measured by eddy covariance and flux–gradient similarity methods. *Atmospheric Chemistry and Physics*, *14*(1), 231–244. https://doi.org/10.5194/acp-14-231-2014

Pastorello, G., Trotta, C., Canfora, E., Chu, H., Christianson, D., Cheah, Y. W., et al. (2020). The FLUXNET2015 dataset and the ONEFlux processing pipeline for eddy covariance data. *Scientific data*, *7*(1), 1–27. https://doi.org/10.1038/s41597-020-0534-3

Porporato, A., Laio, F., Ridolfi, L., & Rodriguez-Iturbe, I. (2001). Plants in water-controlled ecosystems: Active role in hydrologic processes and response to water stress: III. Vegetation water stress. *Advances in Water Resources*, *24*(7), 725–744. https://doi.org/10.1016/S0309-1708(01)00006-9

Reichstein, M., Falge, E., Baldocchi, D., Papale, D., Aubinet, M., Berbigier, P., et al. (2005). On the separation of net ecosystem exchange into assimilation and ecosystem respiration: Review and improved algorithm. *Global Change Biology*, *11*(9), 1424–1439. https://doi.org/10.1111/j.1365-2486.2005.001002.x

Rice, A. H., Pyle, E. H., Saleska, S. R., Hutyra, L., Palace, M., Keller, M., et al. (2004). Carbon balance and vegetation dynamics in an old-growth Amazonian forest. *Ecological Applications*, *14*(sp4), 55–71. https://doi.org/10.1890/02-6006

Rinne, J., Taipale, R., Markkanen, T., Ruuskanen, T. M., Hellén, H., Kajos, M. K., et al. (2007). Hydrocarbon fluxes above a Scots pine forest canopy: Measurements and modeling. *Atmospheric Chemistry and Physics*, *7*(12), 3361–3372. https://doi.org/10.5194/acp-7-3361-2007

Rödig, E., Cuntz, M., Rammig, A., Fischer, R., Taubert, F., & Huth, A. (2018). The importance of forest structure for carbon fluxes of the Amazon rainforest. *Environmental Research Letters*, *13*(5), 054013. https://doi.org/10.1088/1748-9326/aabc61

Royal Society. (2008). Ground-level ozone in the 21st century: Future trends, impacts and policy implications. In: *Science Policy Report* (Vol. 15/08). The Royal Society.

Sasaki, N., Chheng, K., Mizoue, N., Abe, I., & Lowe, A. J. (2016). Forest reference emission level and carbon sequestration in Cambodia. *Global ecology and conservation*, *7*, 82–96. https://doi.org/10.1016/j.gecco.2016.05.004

Silva, S. J., & Heald, C. L. (2018). Investigating dry deposition of ozone to vegetation. *Journal of Geophysical Research: Atmospheres*, *123*(1), 559–573. https://doi.org/10.1002/2017JD027278

SMEAR II. (2021). Retrieved from https://eu-interact.org/field-sites/hyytiala-forestry-reseatch-station-smear-ii/last

Staudt, M., Wolf, A., & Kesselmeier, J. (2000). Influence of environmental factors on the emissions of gaseous formic and acetic acids from orange (Citrus sinensis L.) foliage. *Biogeochemistry*, *48*(2), 199–216. https://doi.org/10.1023/A:1006289120280

Steinbrecher, R., Hauff, K., Hakola, H., & Rössler, J. (1999). A revised parameterisation for emission modelling of isoprenoids for boreal plants. Biogenic VOC emissions and photochemistry in the boreal regions of Europe: Biphorep, Final report, Contract No ENV4-CT95-0022. Air Pollution research report (70), 29–44.

Stockwell, W. R., Kirchner, F., Kuhn, M., & Seefeld, S. (1997). A new mechanism for regional atmospheric chemistry modeling. *Journal of Geophysical Research*, *102*(D22), 25847–25879. https://doi.org/10.1029/97JD00849

Suni, T., Rinne, J., Reissell, A., Altimir, N., Keronen, P., Rannik, U., & Vesala, T. (2003). Long-term measurements of surface fluxes above a Scots pine forest in Hyytiala, southern Finland, 1996-2001. *Boreal Environment Research*, *8*(4), 287–302.

Wagner, A., Bennouna, Y., Blechschmidt, A. M., Brasseur, G., Chabrillat, S., Christophe, Y., et al. (2021). Comprehensive evaluation of the Copernicus Atmosphere Monitoring Service (CAMS) reanalysis against independent observations: Reactive gases. *Elementa: Science of the Anthropocene*, *9*(1), 00171. https://doi.org/10.1525/elementa.2020.00171

Wesely, M. L. (1989). Parameterization of surface resistances to gaseous dry deposition in regional-scale numerical models. *Atmospheric Environment*, *23*, 1293–1304. https://doi.org/10.1016/0004-6981(89)90153-4

Wong, S. C., Cowan, I. R., & Farquhar, G. D. (1979). Stomatal conductance correlates with photosynthetic capacity. *Nature*, *282*(5737), 424–426. https://doi.org/10.1038/282424a0

Yu, Q., Zhang, Y., Liu, Y., & Shi, P. (2004). Simulation of the stomatal conductance of winter wheat in response to light, temperature and CO_2 changes. *Annals of Botany*, *93*(4), 435–441. https://doi.org/10.1093/aob10.1093/aob/mch023

References From the Supporting Information

Fares, S., Matteucci, G., Mugnozza, G. S., Morani, A., Calfapietra, C., Salvatori, E., et al. (2013). Testing of models of stomatal ozone fluxes with field measurements in a mixed Mediterranean forest. *Atmospheric Environment*, *67*, 242–251. https://doi.org/10.1016/j.atmosenv.2012.11.007

Gao, Y., Markkanen, T., Thum, T., Aurela, M., Lohila, A., Mammarella, I., et al. (2016). Assessing various drought indicators in representing summer drought in boreal forests in Finland. *Hydrology and Earth System Sciences*, *20*, 175–191. https://doi.org/10.5194/hess-20-175-2016

Kolari, P., Chan, T., Porcar-Castell, A., Bäck, J., Nikinmaa, E., & Juurola, E. (2014). Field and controlled environment measurements show strong seasonal acclimation in photosynthesis and respiration potential in boreal Scots pine. *Frontiers of Plant Science*, *5*, 717. https://doi.org/10.3389/fpls.2014.00717

Williams, M., Rastetter, E. B., Fernandes, D. N., Goulden, M. L., Wofsy, S. C., Shaver, G. R., et al. (1996). Modelling the soil-plant-atmosphere continuum in a Quercus–Acer stand at Harvard Forest: The regulation of stomatal conductance by light, nitrogen and soil/plant hydraulic properties. *Plant, Cell and Environment*, *19*(8), 911–927. https://doi.org/10.1111/j.1365-3040.1996.tb00456.x